JOURNAL OF AIRCRAFT
Vol. 43, No. 2, March–April 2006

Flutter and Limit-Cycle Oscillations for a Wing-Store Model with Freeplay

Deman Tang* and Earl H. Dowell†
Duke University, Durham, North Carolina 27708-0300

An experimental delta-wing/store model with freeplay has been designed and tested in the Duke wind tunnel. The wing structure is modeled theoretically using von Kármán plate theory that accounts for geometric strain-displacement nonlinearities in the plate wing structure. A component modal analysis is used to derive the full structural equations of motion for the wing/store system. A linear three-dimensional time-domain vortex lattice aerodynamic model including a reduced-order model aerodynamic technique and a slender-body aerodynamic theory for the store are also used to investigate the nonlinear aeroelastic system. The effects of the freeplay gap, the span location of the store, and the initial conditions on the limit-cycle oscillations (LCO) are discussed. The correlations between the theory and experiment are good for the smaller LCO amplitudes, that is, for flow velocities slightly higher than the flutter velocity, but are not good for the larger LCO amplitudes, that is, higher flow velocities. The theoretical model needs to be improved to determine LCO response for larger-amplitude motions.

Nomenclature

a_i, b_j	=	generalized coordinates in x, y directions, respectively
c	=	delta-wing root chord
D	=	delta-wing plate bending stiffness
d	=	nondimensional freeplay gap of the store, δ/h
E	=	Young's modulus
F^β	=	aerodynamic force on the slender body
h	=	delta wing plate thickness
km, kn	=	numbers of vortex elements on delta wing in x, y directions, respectively
kmm	=	total number of vortices on both the delta wing and wake in the x direction
L	=	delta-wing span
M^β	=	aerodynamic moment on the slender body
m	=	delta-wing panel mass/area, $m = h\rho_m$
mxy	=	number of delta-wing modal functions in the x, y plane defining u, v
nxy	=	number of delta-wing modal functions in the z direction defining w
Q^{ij}	=	generalized aerodynamic force
$q, \dot{q}$	=	state-space vector
q_n	=	generalized coordinate in the z direction
R_a	=	size of reduced-order aerodynamic model
t	=	time
U	=	airspeed
U_f	=	critical flutter velocity
U_i, V_j	=	modal functions in x, y directions
u, v	=	in-plane displacements
w	=	plate transverse deflection
X, Y	=	right and left eigenvector matrices of vortex-lattice eigenvalue model
x, y	=	streamwise and spanwise coordinates
Z	=	eigenvalue matrix of vortex-lattice aerodynamic model
z	=	normal coordinate
β	=	store pitch angle
Δp	=	aerodynamic pressure loading on wing
Γ	=	vortex strength
$\underline{\gamma}$	=	reduced vortex strength
$\overline{\Delta p}$	=	nondimensional aerodynamic pressure, $\Delta p/(\rho_\infty U^2)$
Δt	=	time step, $\Delta x/U$
Δx	=	plate element length in the streamwise direction
δ	=	freeplay gap of the store
θ	=	state-space vector of structural deformation
ν	=	Poisson's ratio
ρ_∞, ρ_m	=	air and plate densities
ψ_k	=	transverse modal function in z direction
ω	=	frequency
$(\dot{})$	=	$\mathrm{d}()/\mathrm{d}t$

Received 4 August 2004; revision received 18 February 2005; accepted for publication 18 February 2005.

*Research Associate Professor, Department of Mechanical Engineering and Materials Science.

†William Holland Hall Professor, Department of Mechanical Engineering and Materials Science and Member of the Center for Nonlinear and Complex Systems; and Dean Emeritus, Pratt School of Engineering.

I. Introduction

THEORETICAL and experimental studies of aeroelastic systems with structural freeplay nonlinearity have been made by many authors (see the following references for recent publications[1–6]). In early work at Duke University, a theoretical model for a helicopter blade with a freeplay pitch stiffness nonlinearity in the rotor control system was developed. A wind-tunnel test model for a flexible rotor blade with freeplay pitch stiffness nonlinearity was also designed and tested. The theoretical and experimental results demonstrated limit-cycle oscillations (LCO) and chaotic motion as well as the effects of various initial disturbances on LCO response (see Refs. 7 and 8). A state-space model proposed by Edwards et al.[9] has been used for time simulations of the three-degree-of-freedom aeroelastic typical section airfoil with freeplay in the structural stiffness of the control surface (see Ref. 10), and a harmonic balance method was also used to analyze this nonlinear system (see Ref. 11). An experimental model designed to simulate the three-degree-of-freedom aeroelastic typical section airfoil in two-dimensional, incompressible flow has been developed as well.[10] LCO and chaotic motion were observed for airspeeds substantially below the flutter boundary predicted by linear theory in the absence of freeplay.

A structural freeplay nonlinearity at the attachment points between the wing and the store of a military aircraft might also be of interest and is the subject of the present paper. A limit-cycle oscillation has been observed in flight test for a wing with stores.[12] However, the precipitating physical mechanism still remains to be fully understood. LCO can occur because of the structural nonlinearity at the attachment between the wing and the store, that is, a freeplay gap and/or dry friction damping in the bolt connection. Also the wing geometric structural nonlinearity is another possible

source for the LCO when a sufficiently large deflection occurs. And of course aerodynamic nonlinearities can play an important role as well, but these are not considered in the present work.

For the present studies, a delta-wing experimental model with an external store has been designed. The wing is modeled as a simple plate of constant thickness. The store is modeled as a slender rigid body that contacts the wing through two support points. The fore support point is articulated to the wing, and the aft support point contacts the wing through a spring and freeplay gap. The store is assumed to have motion relative to the wing in only one degree of freedom, that is, in pitch. Thus the store itself is a single-degree-of-freedom system excited by nonlinear forces from the wing through the two support points and the freeplay gap. The wing is modeled using von Kármán plate theory that allows for geometric strain-displacement nonlinearities in the plate wing structure. A component modal analysis[13,14] is used to derive the full structural equations of motion for the wing/store combination system. A linear three-dimensional time-domain vortex-lattice aerodynamic model using a reduced-order model aerodynamic technique[15] and a slender-body aerodynamic theory for the store are also used to investigate the nonlinear aeroelastic system. For the wing-store and wing-alone models without freeplay, theoretical and experimental results have provided a good physical understanding of the flutter and limit-cycle oscillation characteristics (see Refs. 16 and 17).

In this paper, several freeplay gap values are considered, and the effects of the freeplay gap and the span location of store on the flutter and LCO behavior are discussed. To validate the theoretically predicted flutter and limit-cycle oscillation characteristics of the delta-wing/store model, an experimental investigation has been carried out in the Duke wind tunnel.

The literature on wing/store flutter and LCO is recent for the most part. The interesting work of Yang and Zhao[18] and Liu and Chan[19] considers bilinear and trilinear springs for the wing-store attachment and has shown good agreement between theory and experiment. Wing structural nonlinearities were not considered in their work. Thompson and Strganac[20] and Beran et al.[21] have studied theoretically both structural and aerodynamic nonlinearities for wing/store models in forthcoming publications.

II. State-Space Equations

A schematic of the delta-wing-plate/store geometry is shown in Fig. 1, and a photograph of the experimental delta-wing-plate/store model in the wind tunnel is shown in Fig. 2. The aeroelastic structure/fluid state-space equations are described next.

A. Nonlinear Structural Model

The plate wing and store structures can be viewed as separate components that can be analyzed individually and then joined through an appropriate constraint function. The full structural equations of motion based upon the von Kármán plate theory can thus be obtained in a very compact form.

The classical Rayleigh–Ritz approach will be used here. In the Rayleigh–Ritz approach the original displacement variables u, v, w, which are functions of x, y, and t, are expanded in a series of the product of time-dependent modal coordinates and space-dependent global functions. We expand the transverse or out-of-plane displacement w and the in-plane displacements u and v, as follows:

$$u(x, y, t) = \sum_m a_m(t) U_m(x, y) \qquad m = 1 \ldots mxy \tag{1}$$

$$v(x, y, t) = \sum_n b_n(t) V_n(x, y) \qquad n = 1 \ldots mxy \tag{2}$$

$$w(x, y, t) = \sum_k q_k(t) \psi_k(x, y) \qquad k = 1 \ldots nxy \tag{3}$$

where the transverse natural mode function $\psi_k(x, y)$ and the in-plane natural mode functions $U_i(x, y)$ and $V_j(x, y)$ are calculated

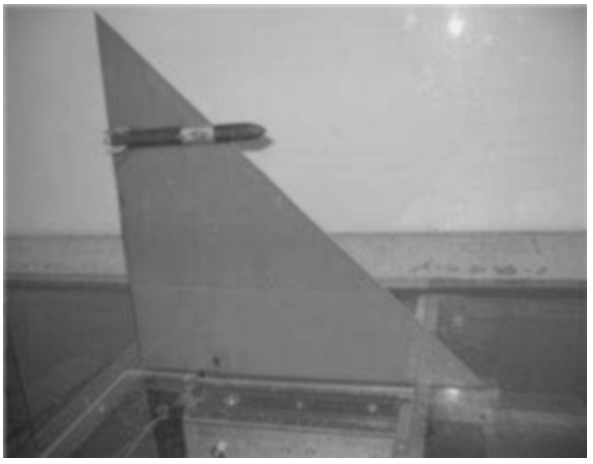

Fig. 2 Photograph of the experimental delta-wing model with an external store in the wind tunnel.

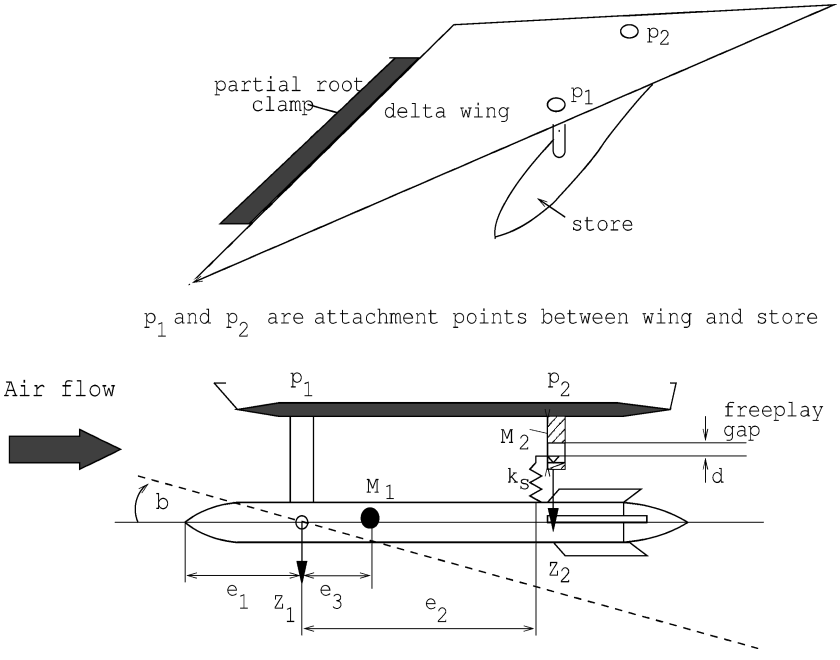

Fig. 1 Delta-wing model with an external store in the wind tunnel.

using a finite element method, that is, a standard computational code ANSYS. These functions satisfy the boundary conditions (partial root clamp) of the cantilevered delta wing.

1. Delta-Wing Plate Energies

Using the mode orthogonality condition, the potential energy of the wing plate is expressed as

$$V^p = \frac{1}{2}\sum_{k=1}^{nxy} m_k \omega_k^2 q_k^2 + \sum_{k=1}^{nxy}\sum_{m=1}^{mxy}\sum_{l=1}^{nxy} S^a_{lmk} a_m q_l q_k + \sum_{k=1}^{nxy}\sum_{n=1}^{mxy}\sum_{l=1}^{nxy} S^b_{lnk} b_n q_l q_k \sum_{k=1}^{nxy}\sum_{r=1}^{nxy}\sum_{s=1}^{nxy}\sum_{t=1}^{nxy} S^q_{rstk} q_r q_s q_t q_k \quad (4)$$

and the kinetic energy is

$$T^p = \frac{1}{2}\sum_{k=1}^{nxy} m_k \dot{q}_k^2 \quad (5)$$

where m_k, ω_k are the generalized mass and natural frequency of the delta wing associated with the kth eigenmode.

The generalized nonconservative work for the wing plate can be expressed as

$$\delta W^p = \sum_{p=1}^{NN}\sum_{k=1}^{nxy} \Delta P_p \psi_k \delta q_k + \sum_{k=1}^{nxy} F^\beta \psi_k(p_1)\delta q_k \quad (6)$$

where ΔP_p is the aerodynamic pressure loading on pth panel that is used to discretely describe the surface of the wing. F^β is the out-of plane (z) force loading on the aft attachment point p_1 of the store.

2. Store Energies

The potential energy of the store is expressed as

$$\begin{cases} V^\beta = \frac{1}{2}k_s(Z_1 + \beta e_2 - Z_2)^2 \\ k_s = \begin{cases} k_{so} & \text{if } |Z_1 + \beta e_2 - Z_2| \geq \delta \\ 0 & \text{otherwise} \end{cases} \end{cases} \quad (7)$$

where k_{so}, δ are the attachment stiffness between the wing and store at the aft attached point and the corresponding freeplay gap, respectively.

The kinetic energy of the store is

$$T^\beta = \tfrac{1}{2}\left(M_1 \dot{Z}_1^2 + M_2 \dot{Z}_2^2 + J_\beta \dot{\beta}^2\right) \quad (8)$$

The generalized nonconservative work for the store can be expressed as

$$\delta W^\beta = M^\beta \delta\beta \quad (9)$$

In Eqs. (7–9) M_1 is the mass of the store, and M_2 is the mass of the aft attachment point; Z_1 and Z_2 are the displacements of the fore p_1 and aft p_2 attachment points of the store, respectively. M^β is a aerodynamic moment loading on the store, and e_2 is the distances between fore and aft attachment points of the store.

The constraint conditions in the fore and aft attached points between the wing and the store can be expressed as

$$f_1 \equiv \sum_{k=1}^{nxy} q_k \psi_k(p_1) - Z_1 = 0 \quad (10)$$

$$f_2 \equiv \sum_{k=1}^{nxy} q_k \psi_k(p_2) - Z_2 = 0 \quad (11)$$

The Lagrangian is

$$L = T - V + \sum_{i=1}^{2} \lambda_i f_i = T^p + T^\beta - V^p - V^\beta + \lambda_1 f_1 + \lambda_2 f_2$$

where λ_i are Lagrange multipliers.

Lagrange's equations for this constrained system are derived with respect to q_k, Z_1, Z_2, λ_1, λ_2, and β to obtain the following six sets of equations:

$$m_k\left[\ddot{q}_k + \omega_k^2 q_k\right] - Q^k - F^\beta + F_N^k = \lambda_1 \psi_k(p_1) + \lambda_2 \psi_k(p_2) \quad (12)$$

$$M_1 \ddot{Z}_1 + k_s(Z_1 - Z_2 + e_2\beta) = -\lambda_1 \quad (13)$$

$$M_2 \ddot{Z}_2 + k_s(Z_2 - Z_1 - e_2\beta) = -\lambda_2 \quad (14)$$

$$J_\beta \ddot{\beta} + k_s e_2^2 \beta + k_s(Z_1 - Z_2)e_2 - M^\beta = 0 \quad (15)$$

$$\sum_{k=1}^{nxy} q_k \psi_k(p_1) - Z_1 = 0 \quad (16)$$

$$\sum_{k=1}^{nxy} q_k \psi_k(p_2) - Z_2 = 0 \quad (17)$$

where F_N^k is a nonlinear force that depends upon the deflection of wing, that is,

$$F_N^k = \sum_{m=1}^{mxy}\sum_{l=1}^{nxy} a_m q_l K1_{mlk} + \sum_{n=1}^{mxy}\sum_{l=1}^{nxy} b_n q_l K2_{nlk} + \sum_{r=1}^{nxy}\sum_{s=1}^{nxy}\sum_{t=1}^{nxy} q_r q_s q_t K3_{rstk}$$

Q^k, F^β, M^β are the generalized aerodynamic forces on the wing and on the store.

Eliminating Z_1, Z_2, λ_1, and λ_2 from the preceding equations, one obtains

$$m_k \ddot{q}_k + M_1 \psi_k(p_1)\sum_{k=1}^{nxy} \ddot{q}_k \psi_k(p_1) + M_2 \psi_k(p_2)\sum_{k=1}^{nxy} \ddot{q}_k \psi_k(p_2) + m_k \omega_k^2 q_k + k_s \Delta\psi_k\left[\sum_{k=1}^{nxy} q_k \Delta\psi_k - e_2\beta\right] = Q^k - F_N^k + F^\beta \psi_k(p_1) \qquad k = 1 \ldots nxy \quad (18)$$

$$J_\beta \ddot{\beta} + k_s e_2^2 \beta - k_s e_2 \sum_{k=1}^{nxy} q_k \Delta\psi_k = M^\beta \quad (19)$$

$$k_s = \begin{cases} k_{so} & \text{if } |\beta e_2 - \sum_{k=1}^{nxy} q_k \Delta\psi_k| \geq \delta \\ 0 & \text{otherwise} \end{cases} \quad (20)$$

where $\Delta\psi_k \equiv \psi_k(p_2) - \psi_k(p_1)$.

Lagrange's equations for this constrained system are also derived with respect to a_m, b_n to obtain the following two sets of equations:

$$\sum_{i=1}^{mxy} a_i A1_{im} + \sum_{j=1}^{mxy} b_j B1_{jm} = \sum_{l=1}^{nxy}\sum_{o=1}^{nxy} q_l q_k C1_{lkm} \qquad m = 1 \ldots mxy \quad (21)$$

$$\sum_{i=1}^{mxy} a_i A2_{in} + \sum_{j=1}^{mxy} b_j B2_{jn} = \sum_{l=1}^{nxy}\sum_{o=1}^{nxy} q_l q_k C2_{lkm} \qquad n = 1 \ldots mxy \quad (22)$$

Note that the store (slender-body) drag is neglected in the present analysis.

B. Aerodynamic Model

1. Vortex-Lattice Model for the Delta Wing

The flow about the wing/store is assumed to be incompressible, inviscid, and irrotational. Here we use an unsteady linear vortex-lattice method to model this flow. The wing and wake are divided into a number of elements. In the wake and on the wing, all of the elements are of equal size Δx in the streamwise direction. Point vortices are placed on the wing and in the wake at the quarter-chord of the elements. At the three-quarter-chord of each panel element, a collocation point is placed for the downwash, that is, the velocity induced by the discrete vortices to set equal to the downwash arising from the unsteady motion of the delta wing. Thus we have the relationship,

$$w_i^{t+1} = \sum_{j}^{kmm} k_{ij} \Gamma_j^{t+1} \qquad i = 1, \ldots, km \tag{23}$$

where w_i^{t+1} is the downwash at the ith collocation point at time step $t+1$, Γ_j is the strength of the jth vortex, and K_{ij} is an aerodynamic kernel function.

An aerodynamic matrix equation is then formed:

$$[A]\{\Gamma\}^{t+1} + [B]\{\Gamma\}^{t} = \{w\}^{t+1} \tag{24}$$

where $[A]$ and $[B]$ are aerodynamic coefficient matrices.

From the fundamental aerodynamic theory, we can obtain the pressure distribution on the plate at the jth point in terms of the vortex strengths. The aerodynamic pressure is given by

$$\Delta P_j = \frac{\rho_\infty}{\Delta x}\left[U \frac{\left(\Gamma_j^{t+1} + \Gamma_j^{t}\right)}{2} + \sum_{i}^{j} \Delta x \frac{\left(\Gamma_i^{t+1} - \Gamma_i^{t}\right)}{\Delta t} \right] \tag{25}$$

and the aerodynamic generalized force is calculated from

$$Q^k = \int\int \Delta p \psi_k \, \mathrm{d}x \, \mathrm{d}y = \sum_{j=1}^{NN} \Delta p_j \psi_k(x_j, y_j) \Delta x \Delta y \tag{26}$$

2. Slender-Body Model for the Store

We follow Bisplinghoff et al.,[22] p. 418, and the final results are follows:

$$F^\beta = Z \int_0^{c_{SB}} \frac{\mathrm{d}F^\beta}{\mathrm{d}x_\beta} \mathrm{d}x_\beta = \rho[\ddot{Z}_1 + U\dot{\beta}] \int_0^{c_{SB}} S \, \mathrm{d}x_\beta + \rho\ddot{\beta} \int_0^{c_{SB}} S[x_\beta - e_1] \, \mathrm{d}x_\beta \tag{27}$$

and

$$M^\beta = \rho U[\dot{Z}_1 + U\beta] \int_0^{c_{SB}} S \, \mathrm{d}x_\beta - \rho\ddot{Z}_1 \int_0^{c_{SB}} S[x_\beta - e_1] \, \mathrm{d}x_\beta - \rho\ddot{\beta} \int_0^{c_{SB}} S[x_\beta - e_1]^2 \, \mathrm{d}x_\beta \tag{28}$$

where $S \equiv$ body cross-section area, $c_{SB} \equiv$ chord of slender body, and e_1 is the distance from learding edge to the elastic axis of the slender body.

Note that

$$\int_0^{c_{SB}} \frac{\mathrm{d}s}{\mathrm{d}x_\beta} \mathrm{d}x_\beta = 0$$

if $S = 0$ at $x_\beta = 0, c_{SB}$, that is, for bodies at both ends.

Also, recall the sign convention is x_β positive aft, F^β positive up, and M^β positive nose up.

For a more detailed derivation of Eqs. (27) and (28), see Ref. 16.

C. Aeroelastic State-Space Equations

Consider a discrete time history of the delta wing $q(t)$ and the store $\beta(t)$ with a constant sampling time step Δt. The structural dynamic equations (20–22) can be reconstituted as a state-space equation in discrete time form, that is,

$$[D_2]\{\theta\}^{t+1} + [D_1]\{\theta\}^{t} + [C_2]\{\Gamma\}^{t+1} + [C_1]\{\Gamma\}^{t} = -\left\{F_N^p\right\}^{t+\frac{1}{2}} + \left\{F_N^\beta\right\}^{t+\frac{1}{2}} \tag{29}$$

where the vector $\{\theta\}$ is the state of the plate, and $\{\theta\} = \{\dot{q}, \dot{\beta}, q, \beta\}$ and $[D_1]$, $[D_2]$ are matrices describing the wing plate and store structural behavior. $[C_1]$, $[C_2]$ are matrices describing the vortex element behavior on the delta wing itself. $\{F_N^p\}$ and $\{F_N^\beta\}$ are the nonlinear force matrices generated by the wing plate structural nonlinearity and the freeplay junction between the wing and store, respectively.

There is a linear relationship between the downwash w at the collocation points and delta-wing response $\{\theta\}$. It is defined by

$$\{w\} = [E]\{\theta\} \tag{30}$$

Thus, combining Eqs. (26), (29), and (30), we obtain a complete aeroelastic state-space equation in matrix form:

$$\begin{bmatrix} A & -E \\ C_2 & D_2 \end{bmatrix} \begin{Bmatrix} \Gamma \\ \theta \end{Bmatrix}^{t+1} + \begin{bmatrix} B & 0 \\ C_1 & D_1 \end{bmatrix} \begin{Bmatrix} \Gamma \\ \theta \end{Bmatrix}^{t} = \begin{Bmatrix} 0 \\ -F_N^p + F_N^\beta \end{Bmatrix}^{t+\frac{1}{2}} \tag{31}$$

III. Reduced-Order Aerodynamic Model

The vortex-lattice aerodynamic model can be "reduced" using aerodynamic eigenmodes.[15] To accomplish this, a transformation from the original flow variables $\{\Gamma\}$ to the modal variables $\{\gamma\}$ is made:

$$\{\Gamma\} = [X_{Ra}]\{\gamma\} \tag{32}$$

where X_{Ra} is composed of the right eigenvectors and Ra is the number of aerodynamic modal vectors kept in the matrix of aerodynamic eigenvectors X. In practice R_a is much less than the dimension of the full vortex-lattice model. $\{\gamma\}$ is the vector of the aerodynamic modal coordinates.

Thus the reduced aeroelastic model has the form

$$\begin{bmatrix} I & -Y_{Ra}^T E \\ C_2 X_{Ra} & D_2 \end{bmatrix} \begin{Bmatrix} \gamma \\ \theta \end{Bmatrix}^{t+1} + \begin{bmatrix} -Z_{Ra} & 0 \\ C_1 X_{Ra} & D_1 \end{bmatrix} \begin{Bmatrix} \gamma \\ \theta \end{Bmatrix}^{t} = \begin{Bmatrix} 0 \\ -F_N^p + F_N^\beta \end{Bmatrix}^{t+\frac{1}{2}} \tag{33}$$

To account for the neglected aerodynamic eigenmodes, we use a quasi-static correction, which accounts for much of their influence. This technique is similar to the mode-acceleration method common to structural dynamics. Finally, the reduced-order model with static correction is given by

$$\begin{bmatrix} I & -Y_{Ra}^T[I - A(A+B)^{-1}]E \\ C_2 X_{Ra} & D_2 + (C_2(A+B)^{-1}E \end{bmatrix} \begin{Bmatrix} \gamma_d \\ \theta \end{Bmatrix}^{t+1} + \begin{bmatrix} -Z_{Ra} & -Y_{Ra}^T B(A+B)^{-1}E \\ C_1 X_{Ra} & D_1 + C_1(A+B)^{-1}E \end{bmatrix} \begin{Bmatrix} \gamma_d \\ \theta \end{Bmatrix}^{t} = \begin{Bmatrix} 0 \\ -F_N^p + F_N^\beta \end{Bmatrix}^{t+\frac{1}{2}} \tag{34}$$

IV. Numerical Results

The theoretical model is a simple delta-wing configuration with a leading-edge sweep of 45 deg and constructed from a 0.147-cm-thick plastic (Lucite). The root chord is partially clamped (cantilevered), and the length of the clamped portion of the root is

22.86 cm (60-percent root chord). The clamping is symmetric about the center of the root chord of the model. The length of the root chord is 38.1 cm. We use the aerodynamic vortex-lattice model including 120 vortex elements on the delta wing ($km = kn = 15$) and 525 vortex elements in the wake ($kmm = 50$) and nine reduced aerodynamic eigenmodes $R_a = 9$. The delta-wing structural modal numbers are $nxy = 10$ in the out-of-plane and $mxy = 200$ in the in-plane directions, respectively. The mesh of the finite element model for the out-of- and in-plane structural model is 30×30, and thus the delta wing is modeled using 900 quadrilateral plate elements. The nodes at the clamped root chord satisfy geometric boundary conditions, that is, $w = u = v = \theta_x = \theta_y = \theta_z = 0$. The first five natural frequencies of the delta-wing plate alone are 4.39, 17.84, 20.62, 42.21, and 51.87 Hz. These results are obtained from a finite element method using a standard code ANSYS.

The store is a slender body attached at the fore and aft support points of the delta wing. The slender body is an plastic tube, 1.59 cm in outside diameter and 13.6 cm in length. A paraboloidal forebody with 2.54 cm length is fixed to the fore end of the tube. The geometry of the paraboloidal forebody is described as follows:

$$R/R_0 = \bar{x}_{\mathrm{SB}}^2, \qquad \bar{x}_{\mathrm{SB}} = 0 \rightarrow 1$$

The slender body is symmetrical. The distance between the fore and aft attachment points is $e_2 = 10$ cm. $J_\beta = 0.4108E_{-4}$ Nms^2, and $k_s = 35{,}77$ N/m. As shown in Fig. 1, $e_1 = 12.7$ cm, and $e_3 = -2.1$ cm. $M_1 = 0.033$ kg, and $M_2 = 0.0055$ kg. As shown in Eqs. (27) and (28).

$$\int_0^{c_{\mathrm{SB}}} S\,\mathrm{d}x_\beta = 3.045E^{-5}\ \mathrm{m}^3, \qquad \int_0^{c_{\mathrm{SB}}} S[x_\beta - e_1]\,\mathrm{d}x_\beta = 4.58E^{-7}\ \mathrm{m}^4$$

and

$$\int_0^{c_{\mathrm{SB}}} S[x_\beta - e_1]^2\,\mathrm{d}x_\beta = 7.657E^{-8}\ \mathrm{m}^5$$

A. Results for the Linear System

In the following calculation we first consider the wing/store structural dynamic behavior as a linear system, that is, the geometric structural nonlinearity of the wing and freeplay in the attachment of wing/store are neglected. In computing the wing/store structural natural frequency, a component modal analysis is used. Only the first 10 wing plate eigenmodes are taken into account in the calculations (out of the total of 961 eigenmodes). A convergence study using various numbers of modes (20, 50, 100, 200, 961) showed that 10 modes give good accuracy for the configuration of interest here. The wing/store structural natural frequency varies with the different points of attachment of wing/store for the leading-edge case. In this case, the fore attachment point (p_1 in Fig. 1) of the wing/store varies along the leading edge of the wing from the nondimensional span $y/c = 0$ (the root chord) to $y/c = 0.7$, and the store chord is always parallel to the root chord. Results are shown in Fig. 3 for the first four wing/store structural natural frequencies vs the nondimensional span location of the store attachment. In this case, the frequencies generally decrease when the store moves from the root to tip of the wing for the first two frequencies and also the fourth frequency. The first mode is dominated by the first wing-alone bending mode. The second mode is dominated by a wing-store mode (note that the store pitch natural frequency alone is 14.63 Hz). The third mode is dominated by the first wing-alone torsion mode. The fourth mode is essentially the second wing-alone bending mode.

The flutter stability of the linearized aeroelastic wing/store model is determined by solving Eq. (34) when the freeplay gap and nonlinear structural force are neglected. The aeroelastic eigenvalues obtained from these equations determine the stability of the system. When the real part of any one eigenvalue λ becomes positive (negative damping), the entire system becomes unstable.

The critical flutter boundary vs nondimensional span location of the store are shown in Fig. 4a for the leading-edge case. The corresponding flutter oscillatory frequencies are shown in Fig. 4b. The critical flutter boundary varies with the span location of the store. The minimum and maximum for the flutter velocity are located

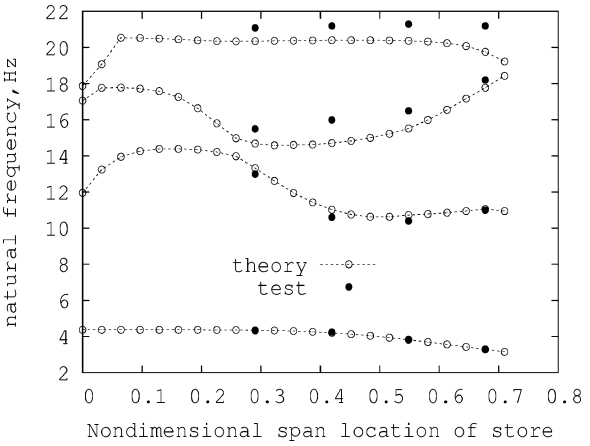

Fig. 3 Wing/store structural natural frequencies vs the nondimensional span location of store attachment for the first four modes.

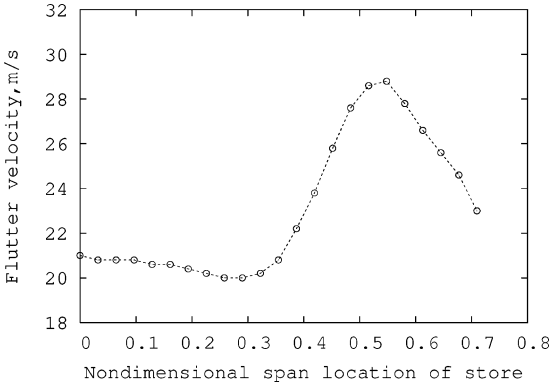

a) Flutter velocity

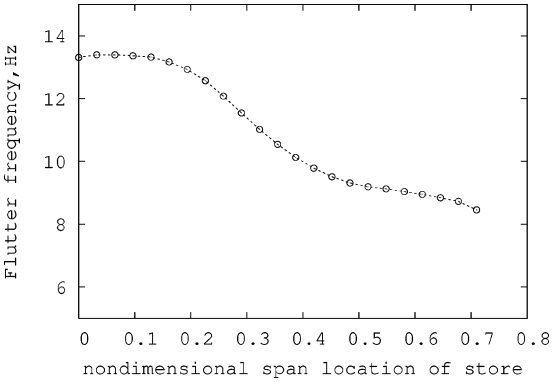

b) Flutter frequency

Fig. 4 Flutter velocity and frequency vs nondimensional span location of store and k_s = 35.77 N/m. No freeplay.

at $y/c = 0.28$ and 0.53, respectively. The flutter frequency decreases as the store moves from the root to the wing tip.

B. Results for the Nonlinear System

Now both the store freeplay nonlinearity and the geometric structural nonlinearity of the wing-store model are considered. Four span locations of the store, $y/c = 0.29, 0.42, 0.55, 0.68$, and four freeplay gap values, $d = \delta/h = 0.0, 1.0, 1.5, 2.0$, are considered in the calculations.

1. Effects of the Freeplay Gap on the LCO Behavior

Figure 5a shows the nondimensional LCO wing-tip amplitude w/h vs the nondimensional flow velocity for the store nondimensional span location $y/c = 0.29$ and various amounts of freeplay. Figure 5b shows the corresponding LCO store pitch angle. Both the LCO wing-tip displacement and store pitch angle are rms values

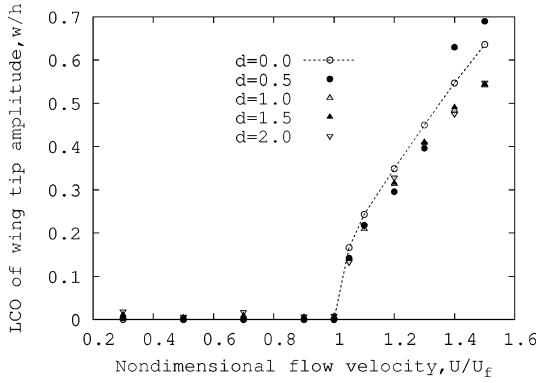

a) Wing-tip response

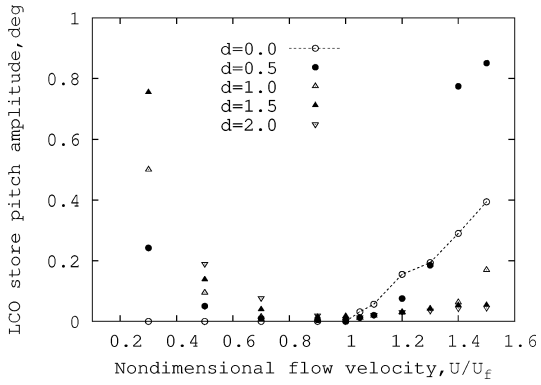

b) Store pitch response

Fig. 5 LCO wing-tip and store pitch amplitudes vs nondimensional flow velocity for the span location of store at *y/c* = 0.29 and various freeplay gaps.

obtained from the steady-state time histories. The nondimensional flow velocity is defined as a ratio of the flow velocity to the linear flutter velocity U/U_f. In the present case, $U_f = 20$ m/s. For comparison, the results for no freeplay case, that is, $d = 0$, are also plotted in these figures. When $U/U_f < 1$, the wing-tip amplitudes are very small, but not zero except for $d = 0$. But the store pitch angle is somewhat larger as shown in Fig. 5b. A small-amplitude LCO for the wing response is found when $U/U_f < 1$. This range is called a preflutter or subcritical LCO. For better understanding this phenomenon, time histories for $U/U_f = 0.5$ and 0.9 are shown. Note that the store pitch amplitude has a complex dependence on flow velocity. To better understand this, consider the following results.

Figure 6a shows the time history of store pitch response for several freeplay gap values and $U/U_f = 0.5$. For $d = 0$, the pitch response is zero. For $d = 0.5$, 1.5, and 2.0, the store has a steady vibration about one equilibrium position, that is, $+0.428$ deg for $d = 0.5$, -1.28 deg for $d = 1.5$ and -1.71 deg for $d = 2.0$. For $d = 1.0$ the store pitch vibration occurs about the two equilibrium positions, -0.856 and $+0.856$. The wing-tip response caused by the store vibration is a complex motion. When the store reaches the equilibrium position, the wing tip has a maximum response, and then the response decays until another impact of the store with the wing occurs as shown in Fig. 6b for $d = 1.0$ and Fig. 6c for $d = 0.5$. The transient decay rate depends the system damping (the structural and aerodynamic damping).

Figure 7a shows the time history of store pitch response for several freeplay gap values and $U/U_f = 0.9$. For $d = 0$, the pitch response is zero (not shown). For other freeplay gap values, the store has a steady vibration about only one equilibrium position (positive). The equilibrium position increases as d increases. A typical wing-tip response for $d = 0.5$ is shown in Fig. 7b. The response is a steady LCO although the motion is small. The fast Fourier transform (FFT) analysis of Fig. 7b is shown in Fig. 7c. The frequency corresponding to the dominant peak amplitude is near the linear flutter frequency, which is not surprising because these results are obtained near the critical flutter state, that is, $U/U_f = 1.0$. The second peak amplitude

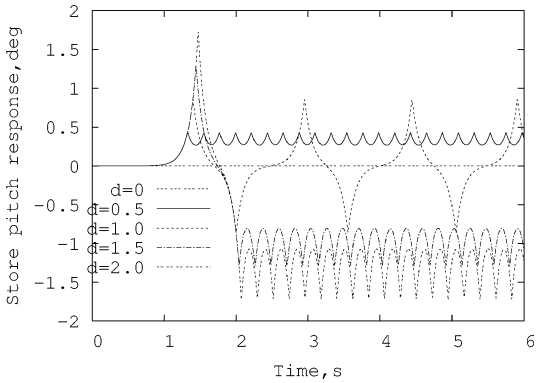

a) Store pitch response for various *d*

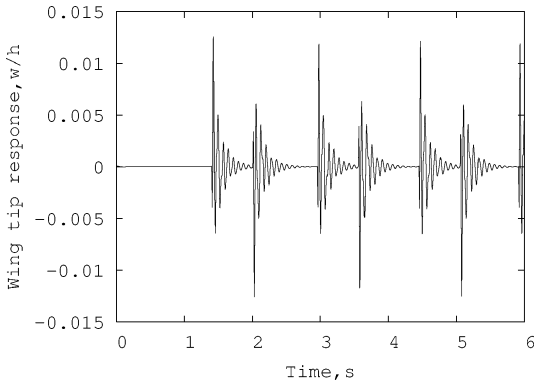

b) Wing-tip response for *d* = 1.0

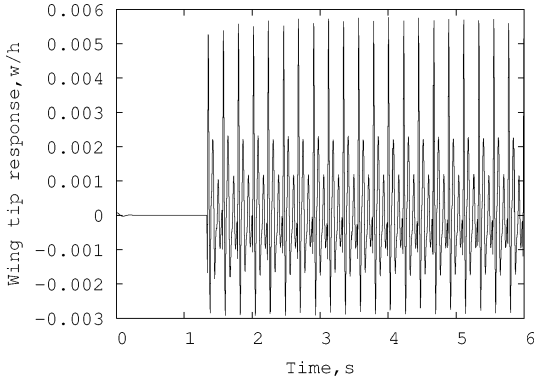

c) Wing-tip response for *d* = 0.5

Fig. 6 Time histories of store pitch and wing-tip response for *U/U_f* = 0.5 and *y/c* = 0.29.

is near the second bending natural frequency of this system for $U/U_f = 0.9$.

Returning to Fig. 5, when the flow velocity is higher than the flutter velocity, that is, $U/U_f > 1$, somewhat different LCO phenomena are observed. This LCO has a large amplitude, and the dominant LCO frequency is close to the frequency for the no-freeplay case. This LCO range is called a postflutter or supercritical LCO. Between the preflutter and postflutter flow velocity ranges, there is a transition flow velocity called U_p or in nondimensional terms U_p/U_f. The nondimensional transition flow velocity U_p/U_f is estimated from Fig. 5 for $y/c = 0.29$ and from Figs. 8–10 for other y/c values. The intersection between the extrapolated supercritical LCO amplitude curve and the flow velocity axis is defined as the transition flow velocity. When the flow velocity is lower than this value, the wing response has a smaller-amplitude LCO; otherwise, a larger-amplitude LCO occurs. For the no-freeplay case, $U_p/U_f = 1$, that is, the transition velocity is equal to the critical flutter velocity, and only supercritical LCO occurs. The wing response is zero for $U_p/U_f \leq 1$, and this flow velocity is usually called the onset flow velocity for LCO to occur.

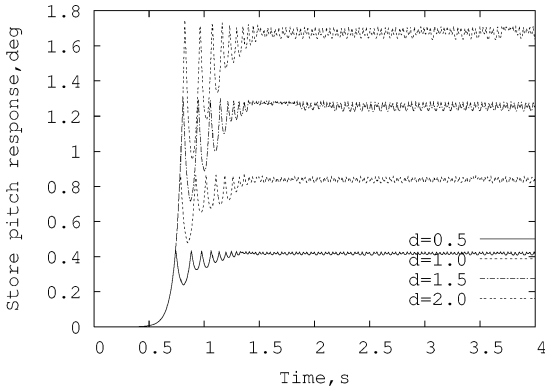

a) Store pitch response for various *d*

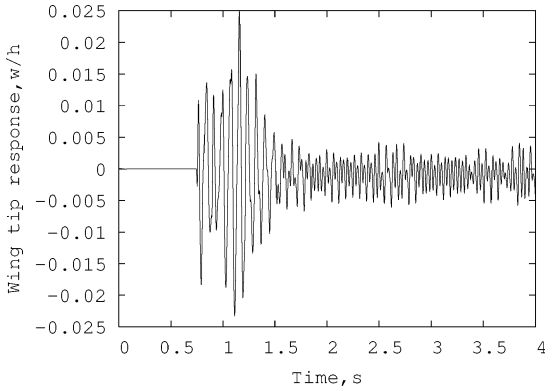

b) Wing-tip response for $d = 0.5$

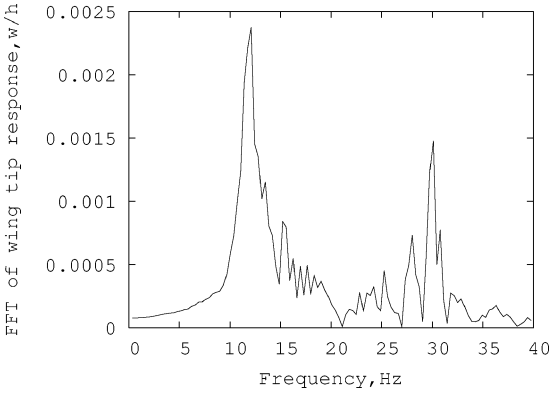

c) FFT analysis of wing-tip response

Fig. 7 Time histories of store pitch and wing-tip response for $U/U_f = 0.9$ and $y/c = 0.29$.

However, in general, the transition flow velocity U_p depends upon the freeplay gap value. For the present case, that is, a span location near the root of the wing, the nondimensional transition velocity U_p/U_f is amost independent of the freeplay gap values, and $U_p/U_f \sim 1$ (see Fig. 5a). When $U_p/U_f > 1$, the wing-tip LCO amplitude increases as the flow velocity increases, and the amplitude can be smaller than that for the no-freeplay case. For more detailed information about the LCO behavior, see the following figures.

Figure 11a shows the time history of store pitch response for several freeplay gap values, and $U/U_f = 1.1$. For $d = 0$, the store pitch response is a steady LCO motion. For other freeplay gap values, the store has a steady vibration only about one equilibrium position (positive). The store pitch motions are similar to those of Fig. 7a, but have a larger LCO amplitude. The results from a FFT analysis of the store pitch motions are shown in Fig. 11b. The LCO frequency is essentially the same as that for the no-freeplay case. A typical wing-tip response for $d = 0.5$ is shown in Fig. 11c. The response motion is a steady LCO with a single harmonic motion even when there is a freeplay gap. Figure 11d shows the results from a FFT

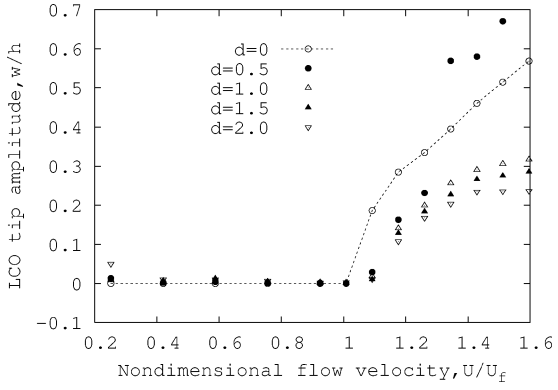

a) Wing-tip response

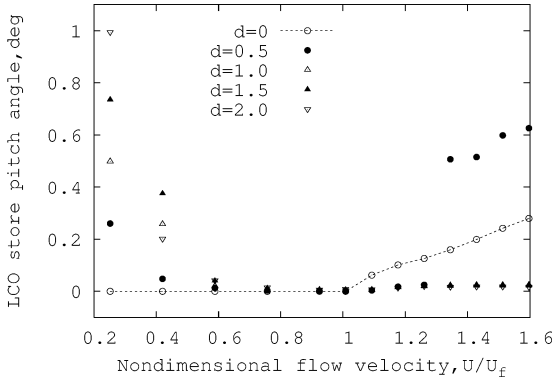

b) Store pitch response

Fig. 8 LCO wing-tip and store pitch amplitudes vs nondimensional flow velocity for the span location of store $y/c = 0.42$ and various *d*.

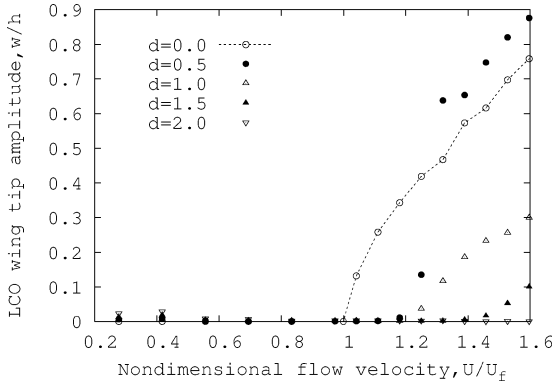

a) Wing-tip response

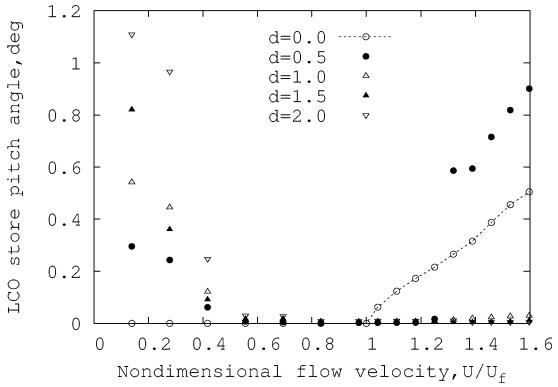

b) Store pitch response

Fig. 9 LCO wing-tip and store pitch amplitudes vs nondimensional flow velocity for the span location of store $y/c = 0.55$ and various *d*.

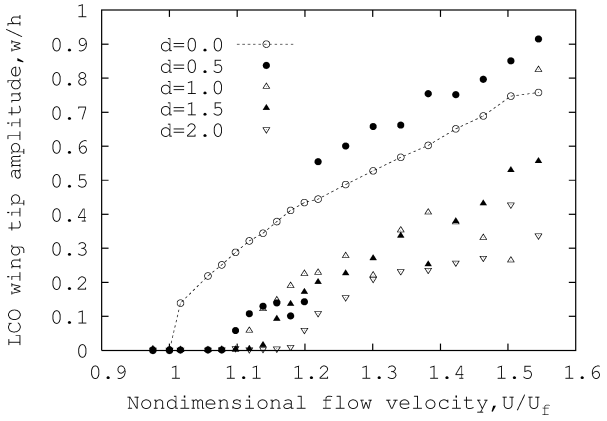

a) Wing-tip response

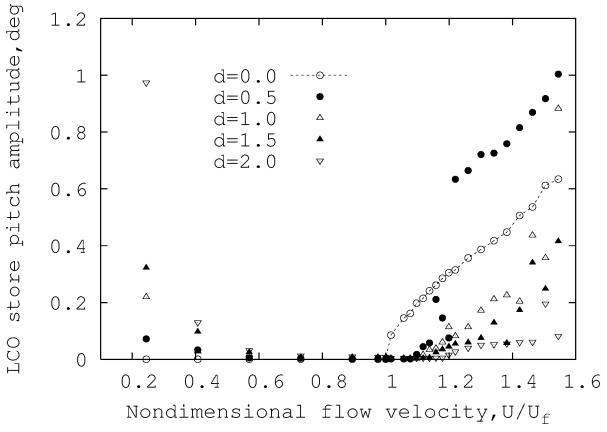

b) Store pitch response

Fig. 10 LCO wing-tip and store pitch amplitudes vs nondimensional flow velocity for the span location of store *y/c* = 0.68 and various *d*.

analysis for the wing-tip response. The results are very close for all freeplay values. This is because the effects of store dynamics and store aerodynamics on the global wing/store LCO are smaller when the span location of store is near the wing root and the flow velocity is near the flutter condition.

Figure 12a shows the time history of store pitch response for several freeplay gap values, and $U/U_f = 1.3$. The store pitch motions are similar to those of Fig. 11a, but have a larger LCO amplitude and response for $d = 0.5$. The store pitch motion for $d = 0.5$ has a chaotic behavior as shown in Fig. 12b in a phase-plane plot of β vs $\dot{\beta}$. There are two rest points for the pitch motion, that is, -0.43 deg and $+0.43$ deg. The response motion is nonperiodic around the two rest points. Results from a FFT analysis of the store pitch motions are shown in Fig. 12c (note the logarithmic scale). For $d = 0$, there is a single harmonic LCO, and the LCO frequency is higher than the peak frequency components for $d \neq 0$. For $d \neq 0$, there is a dominant harmonic peak component, and the higher harmonic components are smaller except for the case of $d = 0.5$. For $d = 0.5$, FFT analysis of the store pitch response reveals a complex response. A typical wing-tip response for $d = 0.5$ is shown in Fig. 12d and a phase-plane plot of w/h vs $\dot{w}/h$ is shown in Fig. 12e. (Note that the dimension of $\dot{w}/h$ is 1/s.) The wing-tip response motion is still a steady LCO with a dominant single harmonic motion and other small harmonic components. Figure 12f shows the results of FFT analysis for the wing-tip response. The results are very similar to those of Fig. 12c, except for $d = 0.5$.

2. Effects of the Store Location on the LCO Behavior

The effects of the store location on the LCO behavior are now considered. The results are shown in Figs. 8a–10a for the nondimensional LCO wing-tip amplitude w/h vs the nondimensional flow velocity at the store nondimensional span locations, $y/c = 0.42$, 0.55, and 0.68, respectively. Figures 8b–10b show the corresponding LCO store pitch angle. As shown in Figs. 8a and 8b for $y/c = 0.42$, the nondimensional transition flow velocity U_p/U_f varies with the freeplay gap values, that is, $U_p/U_f = 1$ for $d = 0$, 1.06 for $d = 0.5$, 1.08 for $d = 1.0$, 1.09 for $d = 1.5$ and 1.095 for $d = 2.0$. Thus, when

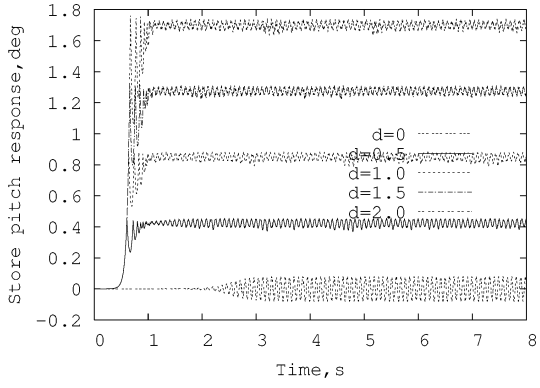

a) Store pitch response for various *d*

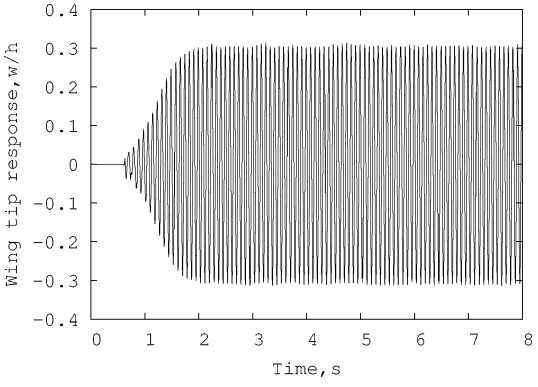

c) Wing-tip response for *d* = 0.5

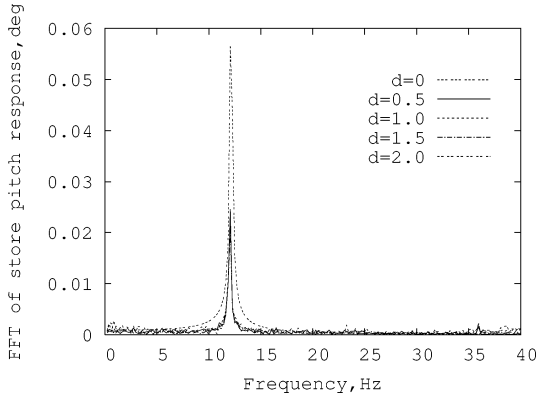

b) FFT analysis of store pitch response for various *d*

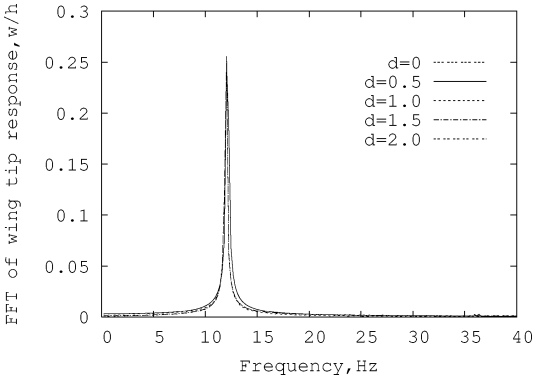

d) FFT of wing-tip response for various *d*

Fig. 11 Time histories and FFT analysis for the store pitch and wing-tip response for $U/U_f = 1.1$ and *y/c* = 0.29.

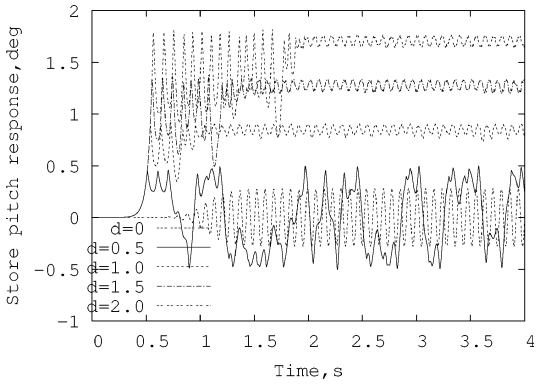

a) Store pitch response, various d

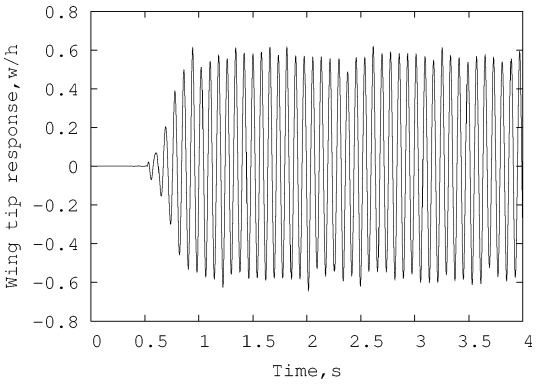

d) Wing-tip response for $d = 0.5$

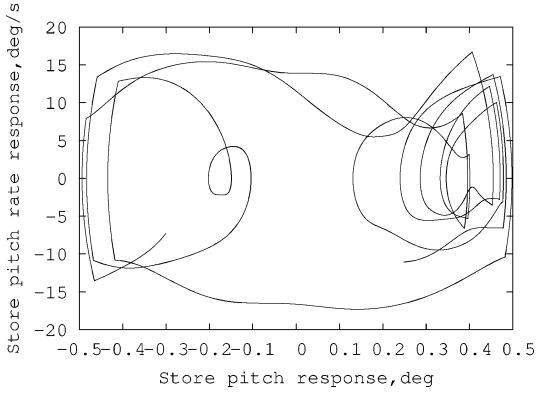

b) β vs β for $d = 0.5$

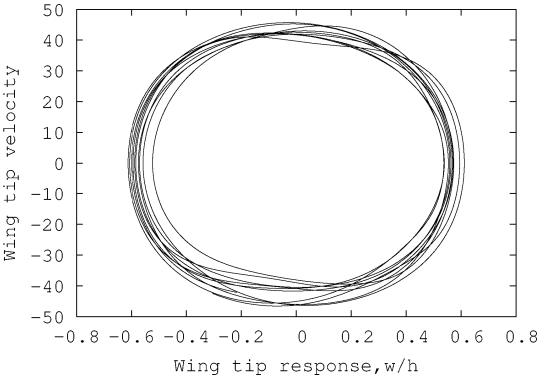

e) $\dot{w}/h$ vs w/h for $d = 0.5$

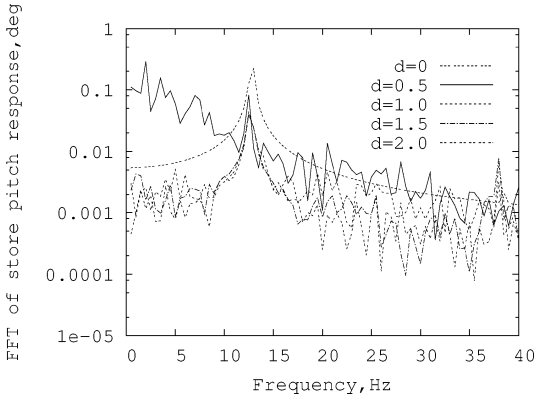

c) FFT of store pitch response for various d

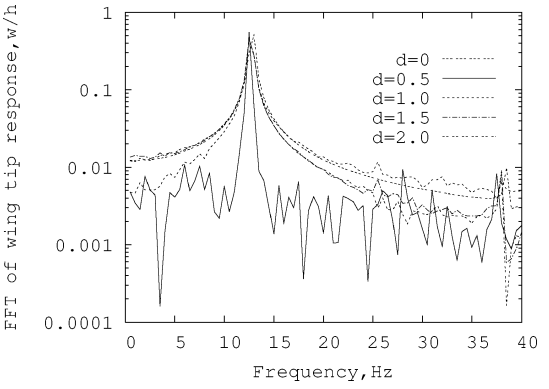

f) FFT analysis of wing-tip response for various d

Fig. 12 LCO behavior of the store pitch and wing-tip response for $U/U_f = 1.3$ and $y/c = 0.29$.

the freeplay gap increases the onset velocity of the postflutter LCO (large LCO amplitude range) increases. In the postflutter LCO range, the LCO amplitude for $d \neq 0$ is smaller than that for $d = 0$ except $d = 0.5$ and $U/U_f > 1.32$. For $d = 0.5$ and $U/U_f > 1.32$, the store pitch response motion is larger, and there is a periodic or nonperiodic vibration around the two equilibrium or rest positions. It is found that the effects of the store location on the LCO behavior are significant.

As shown in Figs. 9a and 9b for $y/c = 0.55$, the transition flow velocity can be larger than the critical flutter velocity. The nondimensional transition velocity U_p/U_f is 1 for $d = 0$, 1.18 for $d = 0.5$, 1.22 for $d = 1$, 1.45 for $d = 1.5$ and 1.8 for $d = 2.0$ (not shown in this figure). In this case, the freeplay gap significantly delays the onset of the postflutter LCO, and the LCO amplitude for $d \neq 0$ is smaller than that for $d = 0$ except for $d = 0.5$ and $U/U_f > 1.27$, where the store pitch amplitude is relatively larger. Recall the preceding discussion for the cases of $y/c = 0.29$ and 0.42.

Figures 10a and 10b show the LCO wing-tip amplitude and store pitch angle vs nondimensional flow velocity for $y/c = 0.68$. Here the emphasis is on the postflutter range, and the results for $U/U_f < 0.9$ are not shown in Fig. 10a. The nondimensional transition velocity U_p/U_f for the postflutter LCO range is 1 for $d = 0$, 1.077 for $d = 0.5$, 1.09 for $d = 1.0$, 1.17 for $d = 1.5$ and 1.16 for $d = 2.0$. There are three flow velocity ranges, and these are discussed next.

When $U/U_f < 1$, the wing LCO amplitude is relatively small, and the motion is complex, although the store pitch angle is large and the motion has a chaotic behavior. Time histories of store pitch response for $d = 0.5$ and 2.0 for $U/U_f = 0.23$ are shown in Figs. 13a and 13b. The store pitch vibration is around two equilibrium positions. Although the pitch amplitude is large, the wing LCO response is small as shown in Figs. 13c and 13d. The responses are similar to Figs. 6b and 6c for $d = 1.0$ and 0.5.

Summarizing the results of Fig. 6 for $y/c = 0.29$ (store is near the wing root) and Fig. 13 for $y/c = 0.68$ (store is near the wing tip), the LCO behavior in the preflutter LCO range is almost identical for the different y/c values. Of course, these relatively small LCO motions can still present a fatigue problem for an aircraft.

When $1 < U/U_f < U_p/U_f$, the store has a steady vibration around one equilibrium position, and the LCO amplitude is smaller than the results for the no-freeplay case. A typical time history for $U/U_f = 1.05$ is shown in Fig. 14a. The corresponding wing-tip

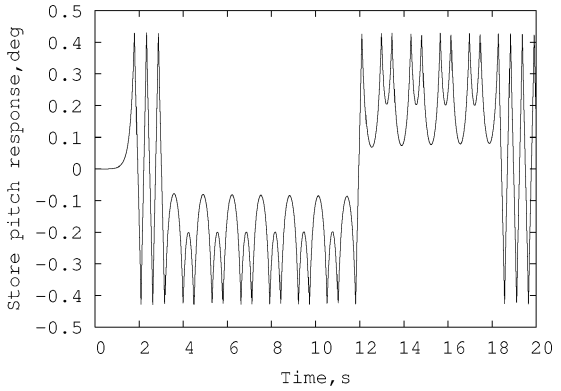

a) Store pitch response for $d = 0.5$

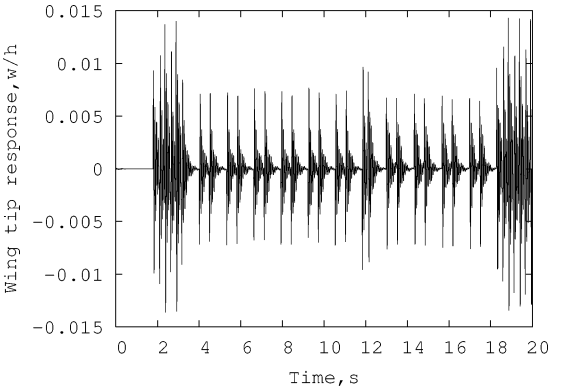

c) Wing-tip response for $d = 0.5$

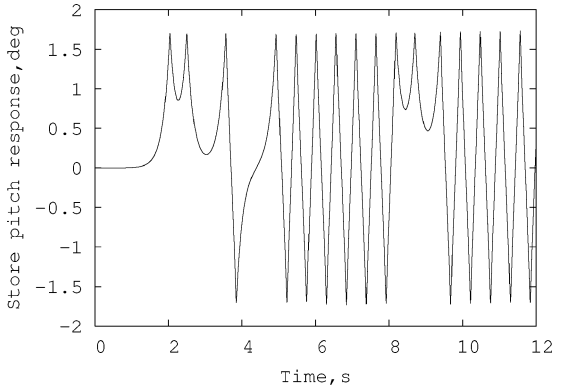

b) Store pitch response for $d = 2.0$

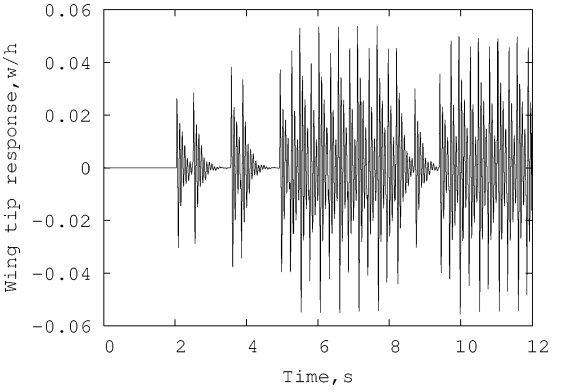

d) Wing-tip response for $d = 2.0$

Fig. 13 Time histories for the store pitch and wing-tip response for $U/U_f = 0.23$ and $y/c = 0.68$ for various d.

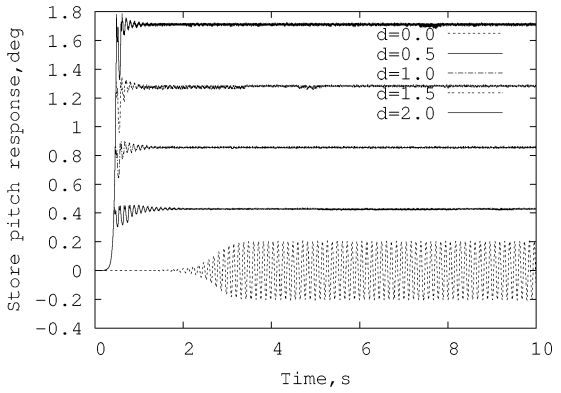

a) Store pitch response for various d

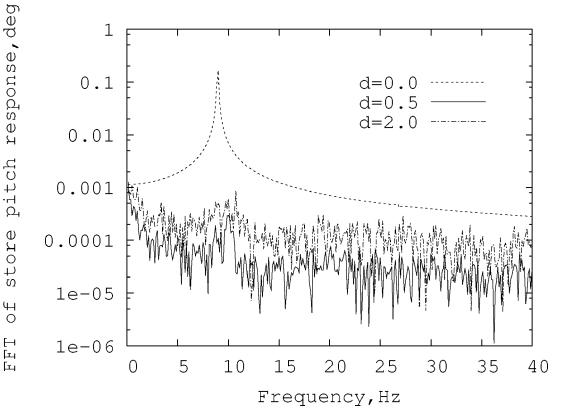

c) FFT analysis of store response

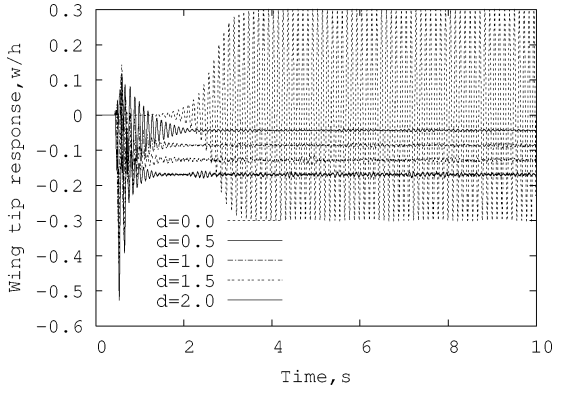

b) Wing-tip response for various d

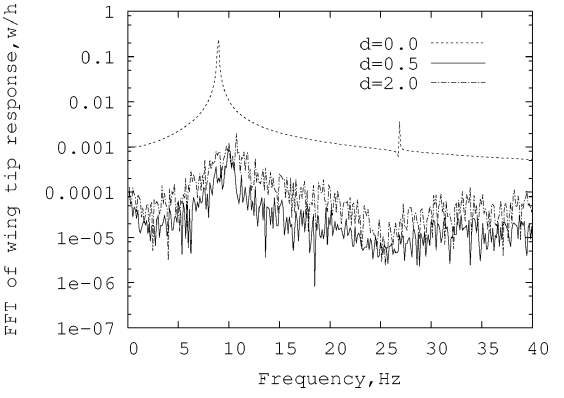

d) FFT analysis of wing-tip response

Fig. 14 Time histories and FFT analysis of the store pitch and wing-tip response for $U/U_f = 1.05$ and $y/c = 0.68$ for various d.

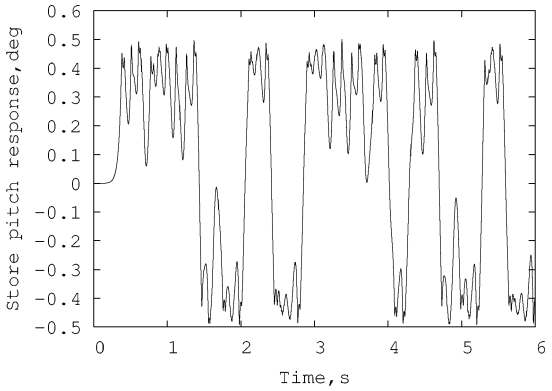

a) Store pitch response

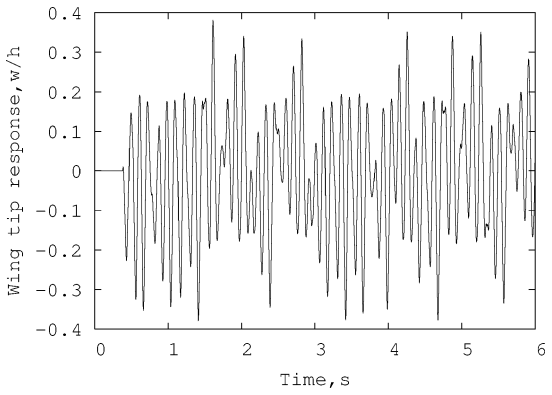

b) Wing-tip response

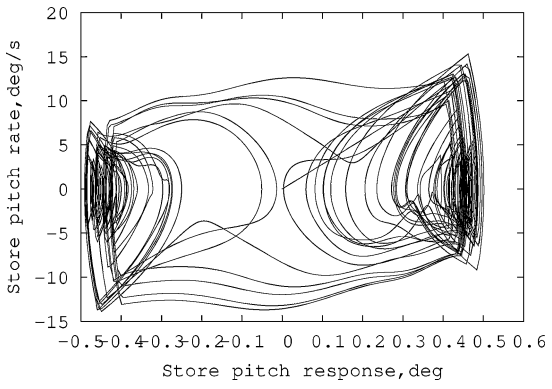

c) $\dot{\beta}$ vs β

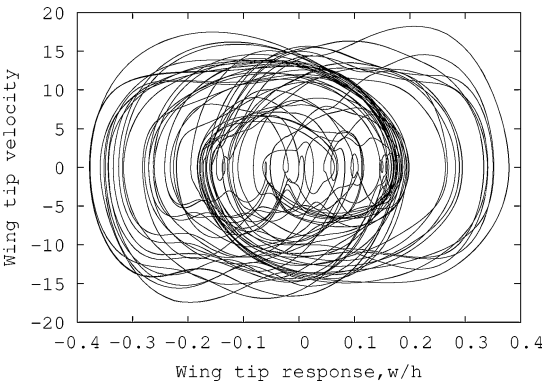

d) $\dot{w}/h$ vs w/h

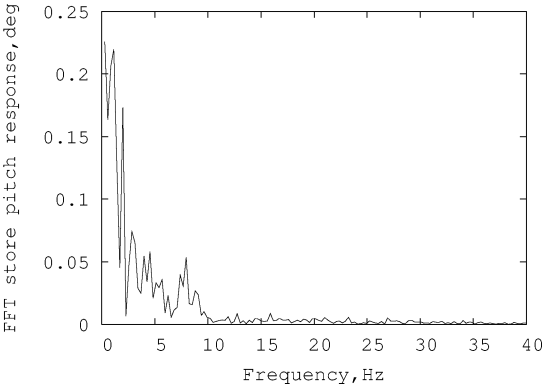

e) FFT of store pitch response

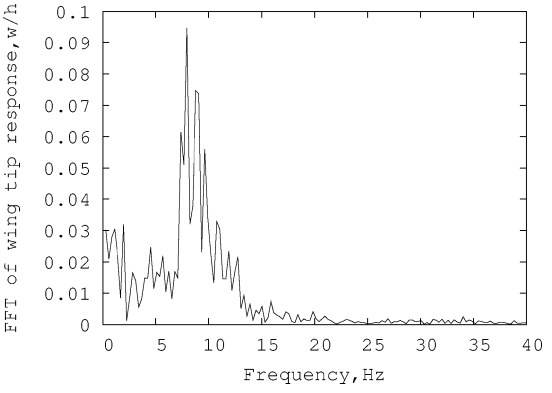

f) FFT of wing-tip response

Fig. 15 LCO behavior of the store pitch and wing-tip response for $U/U_f = 1.2$, $d = 0.5$, and $y/c = 0.68$.

vibration is around a static equilibrium position for a given freeplay gap value. The wing LCO amplitude is still small as shown in Fig. 14b. Results from a FFT analysis for both the store pitch and wing-tip responses are shown in Figs. 14c and 14d. For the wing-tip response, there is still a dominant frequency component, and the frequency is slightly higher than the LCO frequency for the no-freeplay case.

When $U/U_f > U_p/U_f$, larger LCO amplitudes for both the wing-tip and store pitch response are observed. Usually, the wing LCO amplitude is smaller than that for $d = 0$; see $U/U_f < 1.2$ in Fig. 10a. However, there is a jump phenomenon for a certain flow velocity and freeplay gap. After the "jump," the wing-tip LCO amplitude is larger than that for $d = 0$. As shown in Fig. 10, the nondimensional jump flow velocity is 1.22 for $d = 0.5$ and 1.54 for $d = 1.0$. The onset of the jump phenomenon depends upon the store pitch response. To better understand the jump phenomenon, consider the following results.

Figure 15a shows a time history of the store pitch response for $U/U_f = 1.2$ and $d = 0.5$ (below the jump flow velocity). The store has a steady vibration around two equilibrium positions, and the LCO pitch amplitude is larger. The motion is chaotic as shown in Fig. 15c for the phase plane plot of $\dot{\beta}$ vs β. The corresponding wing-tip response is shown in Fig. 15b, and the phase plane plot of $\dot{w}/h$ vs w/h is shown in Fig. 15d. The motion is complex and chaotic, but the LCO amplitude is not large. Results from a FFT analysis for both the store pitch and wing-tip responses are shown in Figs. 15e and 15f. There is a relatively broad frequency bandwidth response near the LCO frequency for the no-freeplay case, and the energy spectrum for the lower frequency components is not small.

Figure 16a shows typical time histories of store pitch response for $d = 0, 0.5, 2.0$ at $U/U_f = 1.22$ (jump velocity). For $d = 1.0$ and 1.5, the store pitch motions are similar to those for $d = 2.0$, but they are about different equilibrium positions. For $d = 0.5$, the steady-state motion is a periodic vibration with a larger amplitude. Results from the corresponding FFT analysis are shown in Fig. 16b. It is found that the LCO frequency is 10.37 Hz for both $d = 0.5$ and 2.0, but 9.22 Hz for $d = 0$. Figures 16c and 16d show a typical time history of wing-tip response for $d = 0.5$ and the corresponding results from a FFT analysis for $d = 0, 0.5, 2.0$. Recalling Fig. 15a (below the jump velocity) and Fig. 16a (at the jump velocity), it is found that when

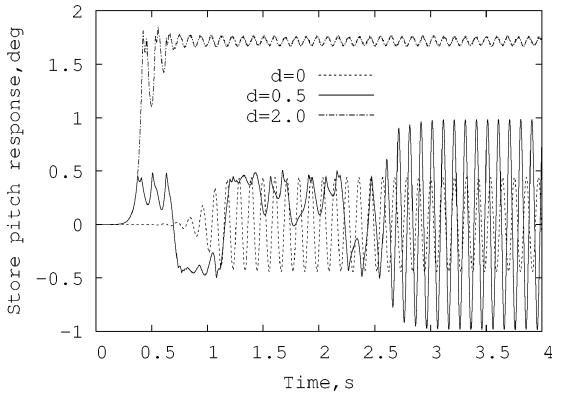

a) Store pitch response

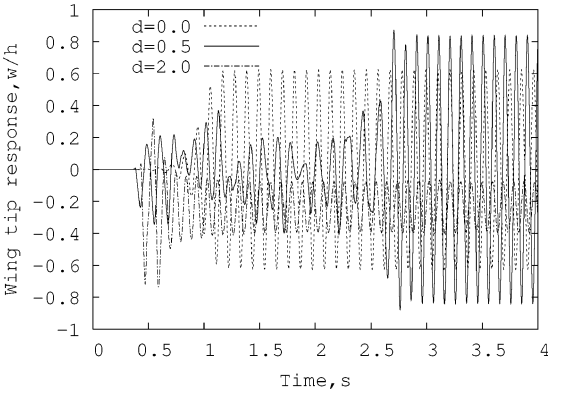

c) Wing-tip response for $d = 0.5$

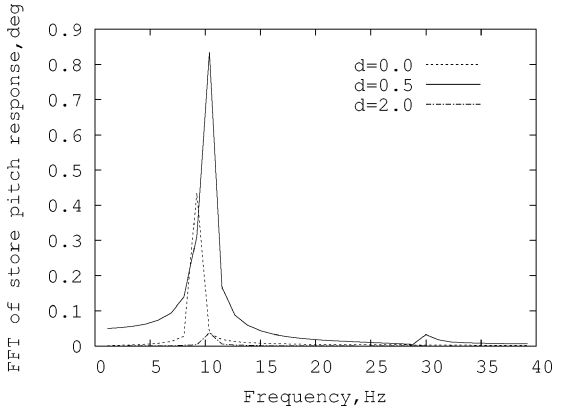

b) FFT analysis of store pitch response

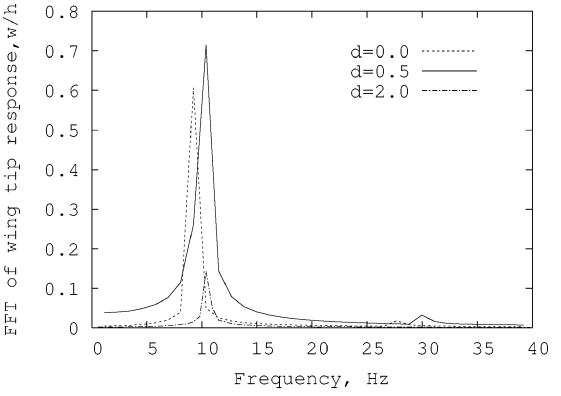

d) FFT analysis of wing-tip response

Fig. 16 Time histories and FFT analysis for the store pitch and wing-tip response for $U/U_f = 1.22$ and $y/c = 0.68$ for various d.

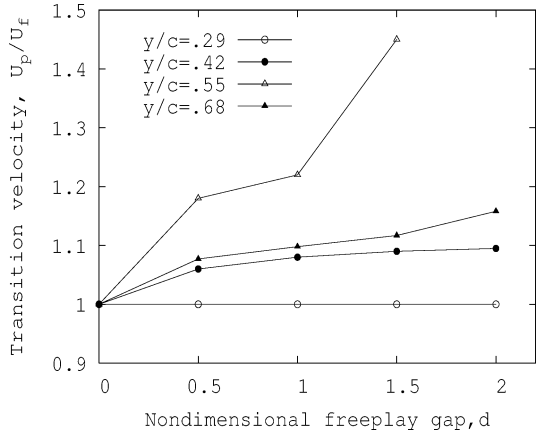

Fig. 17 Nondimensional transition velocity vs freeplay gap values for several span locations of store.

the flow velocity is higher than that where the store pitch motion becomes a periodic vibration with a large amplitude (around two equilibrium positions), the wing-tip LCO response reveals a jump phenomenon, and the LCO amplitude is larger than that for the no-freeplay case. The freeplay nonlinearity changes the original wing/store structural characteristics and the LCO behavior.

Summarizing the results of Figs. 11 and 12 for $y/c = 0.29$ and Fig. 15, Fig. 16 for $y/c = 0.68$, the LCO response in the postflutter LCO range has a larger amplitude and a dominant frequency that is close to that of the no-freeplay case. The wing LCO amplitude is significantly dependent on the store pitch motion.

For the supercritical LCO range, the effects of the store location on the change in nondimensional transition flow velocity vs the freeplay gap are shown in Fig. 17. When the store is near the wing root, U_p/U_f is almost 1, and independent of the freeplay gap values, see the results for $y/c = 0.29$. This means the effect of the store aerodynamics and structural dynamics is relatively small. When the store is near wing tip, U_p/U_f increases as the freeplay gap value increases; see the results for $y/c = 0.68$. The effect of the store aerodynamics and structural dynamics is now larger. When the store is near the position where the system has a maximum flutter velocity (recall Fig. 4a), U_p/U_f is most sensitive to the freeplay gap value; see the results for $y/c = 0.55$. The effect of the store aerodynamics and structural dynamics is most significant in this case.

3. *Effects of the Initial Conditions on the LCO Behavior*

In Secs. IV.B.1 and IV.B.2, all results were obtained from the following initial conditions: the nondimensional wing-tip displacement is $w(0)/h = 0.001$, and the wing displacement at other points on the wing, the store pitch angle $\beta(0)$ and the reduced vortex strength $\gamma(0)$ are zero, which is called case I.C.1. In this case, the wing and store pitch initial displacement conditions are small, that is, $|\beta(0)e_2 + Z_1(0) - Z_2(0)| < \delta$. In this section, the effects of the larger initial conditions, that is, $|\beta(0)e_2 + Z_1(0) - Z_2(0)| > \delta$, on the LCO behavior are considered. Two typical initial conditions are used in the calculations:

1) The initial store pitch angle $\beta(0) = 0.5$ deg, but all wing displacements and the others are zero, which is called case I.C.2. Note that the static equilibrium position of the store for $d = 0.5$ is 0.428 deg.

2) The initial store pitch angle $\beta(0) = 1.0$ deg, but all wing displacements and the others are zero, which is called case I.C.3. Note that the static equilibrium position of the store for $d = 1.0$ is 0.856 deg.

Figure 18 shows the LCO wing-tip amplitude vs the flow velocity for $y/c = 0.68$ and no freeplay, that is, $d = 0$. The LCO amplitude is essentially independent of the initial conditions.

Figures 19a and 19b show the LCO wing-tip amplitude and store pitch angle vs the flow velocity for $y/c = 0.68$ and $d = 0.5$. For the initial conditions of case I.C.1, the results were shown in Fig. 10.

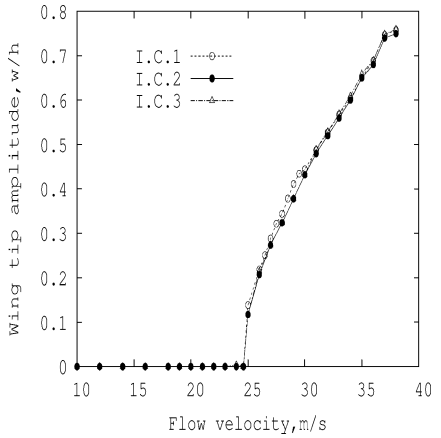

Fig. 18 LCO wing-tip amplitude vs the flow velocity for $y/c = 0.68$ and the no-freeplay case.

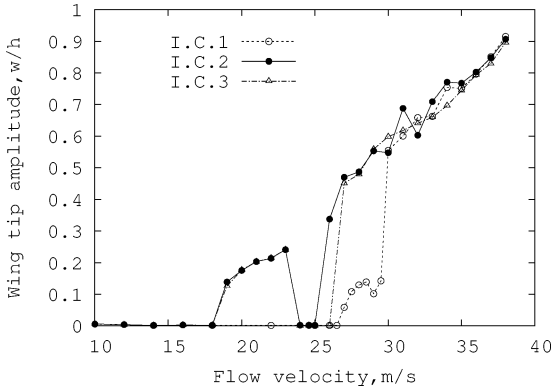

a) Wing-tip response

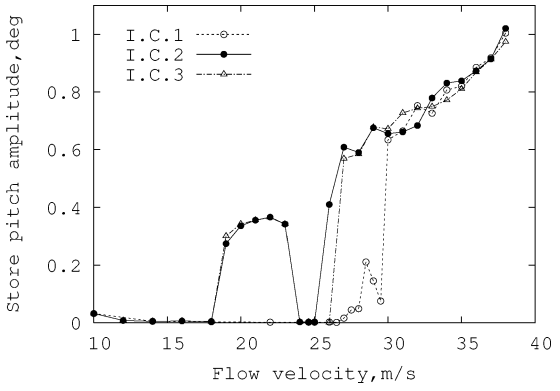

b) Store pitch response

Fig. 19 LCO wing-tip and store pitch amplitudes vs flow velocity for the span location of store, $y/c = 0.68$, $d = 0.5$, and various initial conditions.

The jump flow velocity is 30 m/s, that is, $U_p/U_f = 1.22$. There is a chaotic LCO range with moderate amplitudes from $U = 27$ to 29 m/s. For the initial conditions of case I.C.2, the initial pitch angle is slightly larger than the static equilibrium position of the store for $d = 0.5$. There are two jump flow velocities from the smaller LCO to the larger LCO. The first is $U = 19$ m/s, and the second is $U = 26$ m/s. Between the first and second jump flow velocities, there is a smaller amplitude LCO range from 24 to 25 m/s. For the initial conditions of case I.C.3, the initial pitch angle is substantially larger than the static equilibrium position of the store for $d = 0.5$. The results are similar to those for the case I.C.2, but the second jump velocity is now 27 m/s. When $U > 30$ m/s, the LCO amplitudes are almost the same using any of the different initial conditions. The transition flow velocity U_p is lower than the flutter velocity $U_p/U_f = 0.79$ and 1.07 for case I.C.2 and $U_p/U_f = 1.1$ for case

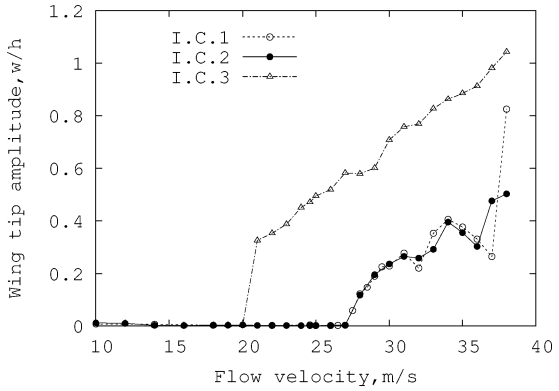

a) Wing-tip response

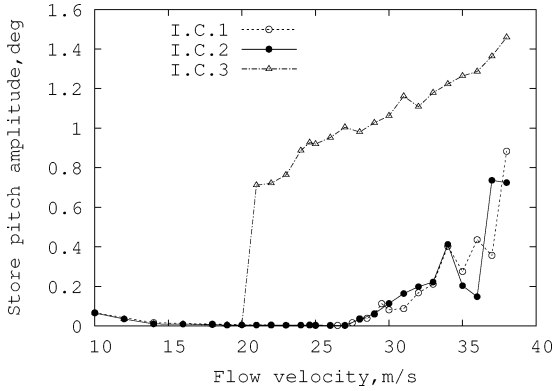

b) Store pitch response

Fig. 20 LCO wing-tip and store pitch amplitudes vs flow velocity for the span location of store, $y/c = 0.68$, $d = 1.0$, and various initial conditions.

I.C.3. These results are also found from Fig. 19b that shows the store pitch angle vs the flow velocity.

When the freeplay gap value increases from $d = 0.5$ to 1.0, the results are shown in Figs. 20a and 20b for the LCO wing-tip amplitude and store pitch angle vs the flow velocity. The LCO amplitudes for cases I.C.1 and I.C.2 are quite close, but are very different for case I.C.3. The transition flow velocity U_p is 27 m/s for both cases I.C.1 and I.C.2, but is 21 m/s for case I.C.3, and the LCO amplitude becomes large.

As shown in Fig. 19, the jump flow velocity depends upon both the initial conditions and the flow velocity, that is, the dynamic equilibrium condition. Figures 21a and 21b show the wing-tip LCO amplitude and the store pitch angle vs the initial store pitch angle (the wing initial displacements and the initial reduced vortex strength are zero) for various d at a flow velocity of 26 m/s. For no freeplay ($d = 0$), the wing-tip LCO amplitude is independent of the initial store pitch angle. For $d = 0.5$ the LCO jump occurs when the initial store pitch angle is between $\beta(0) = 0.47$–0.55 deg, and for $d = 1.0$ the corresponding initial store pitch angle is between $\beta(0) = 0.95$–1.2 deg. It is seen that there is a relatively broader range of initial store pitch angle that leads to larger LCO amplitudes for the larger freeplay gap.

Summarizing the results of Figs. 18–21 for $y/c = 0.68$, the LCO behavior is sensitive to the initial store pitch angle. LCO response with a large amplitude can occur at a flow velocity below the flutter velocity when the initial store pitch angle reaches a certain threshold value.

V. Theoretical and Experimental Flutter/LCO Correlations

The experimental delta wing and the store configuration parameters are the same as those of the theoretical model. The store pitch stiffness k_s is 35.77 N/m, and corresponding store pitch natural frequency is 14.63 Hz. A steel leaf spring is inserted tightly into the store body near the fore support (articulated point). The free end

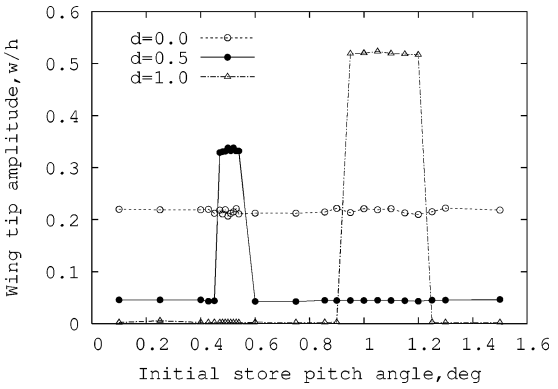

a) Wing-tip response

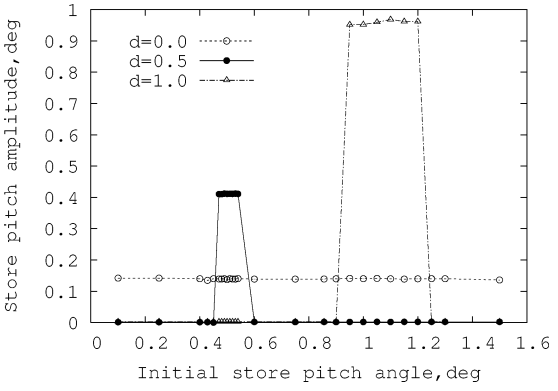

b) Store pitch response

Fig. 21 LCO wing-tip and store pitch amplitudes vs initial store pitch angle (the others are zero) for various d at a flow velocity of 26 m/s.

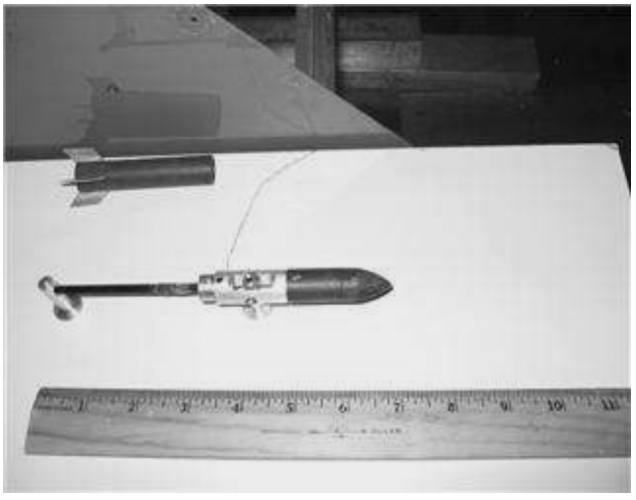

Fig. 22 Photograph of the experimental store model.

of the leaf spring is attached to the aft support point with a certain freeplay gap value. Two strain gauges are glued to both sides near the fixed end of the leaf-spring and are used to measure the store pitch angle. The dynamic calibration coeffecient was determined by a ground-vibration test. A photograph of the store pitch measurement and the leaf spring-freeplay configuration is shown in Fig. 22.

The natural frequencies of wing/store structural model were determined by measuring the transfer function of input force and output acceleration. A force transducer B&K 8200 fixed near the wing root is excited by a minishaker B&K 4810 and a power amplifier B&K 2706. A four-channel signal analyzer (SD 380) provides a sweeping sinusoidal signal. The output signal from a microaccelerometer (at wing tip) provides inputs to the SD380 for transfer function analysis. The experimental results for the first four natural frequencies are shown in Fig. 3 as indicated by the symbol of •. The agreement for the first two natural frequencies is excellent and for the third and fourth natural frequencies is reasonably good.

A typical span location of the store for the leading-edge case $y/c = 0.68$ (near the wing tip) and two freeplay gap values $d = 0.5$ and 1.0 are considered in the experiment. A microaccelerometer is fixed on the wing mid-span of the trailing edge. The LCO acceleration amplitude is measured from this transducer. The calibration coeffecient is $s_a = g/v$, where g is the gravity acceleration, $g = 9.81$ m/s^2. A data-acquisition system, LabView 5.1 version, is used to obtain the measurement data. The sampling rate is 500 points/s, $\Delta t = 1/500$, and the total sampling length is 5000 points. An ensemble-averaged FFT analysis is used to determine LCO frequency using a time-delay average method. The delay time is $2 \times \Delta t$, and the FFT analysis uses 2048 sampling points. The ensemble average number is 100. A rms acceleration amplitude is used to represent the correlations between the theory and experiment. The experimental rms acceleration amplitude is obtained from the time history over 5000 sampling points.

When the flow velocity is higher than the flutter velocity, LCO behavior is observed experimentally. Typical measured time histories are shown in Figs. 23a and 23b for $U = 26.3$ m/s, $d = 0.5$ and Figs. 24a and 24b for $U = 25.98$ m/s, $d = 1$, where Fig. 23a is for LCO acceleration response at the wing midspan of the trailing edge and Fig. 23b is for the store pitch response. (Note the flutter velocity is 24.4 m/s.) Corresponding to Figs. 23 and 24, the results from FFT analyses are shown in Figs. 23c and 23d and Figs. 24c and 24d. For comparison with the experimental results, the theoretical results are also plotted in these figures. Note that for the theoretical results of Fig. 23 the initial condition, I.C.2 case, is used and for Fig. 24, the I.C.3 case is used.

As shown in Figs. 23b and 24b for the measured store pitch response, the store pitch angle scaling is calibrated by the linear system, that is, for no freeplay. With freeplay, this scale is not precisely accurate because in the freeplay range the strain of the leaf-spring is zero. The error is at least 0.428 deg for $d = 0.5$ and 0.856 deg for $d = 1$. Hence, such a measurement method using the strain gauges to measure the freeplay pitch angle is not entirely successful. The present measured store pitch data only provide qualitative information.

As shown in Figs. 23a and 23b, there is a "beat" phenomenon and an impact in the acceleration LCO response. This is because of the unsteady store pitch motion when there is a freeplay gap. The FFT analysis shows the dominant frequency is 8.8 Hz for the experiment and 10 Hz for the theory. The agreement between the theory and experiment is reasonable. There are some higher harmonic frequency components in Figs. 23c and 23d. The higher harmonic frequency component seen in the theoretical model (but not in the experiment) at 30 Hz is caused by the wing geometrical structural nonlinearity. Similar results are shown in Fig. 24 for $U = 25.98$ m/s and $d = 1$.

Figures 25a and 25b show the theoretical and experimental LCO acceleration amplitude at the wing midspan and the store pitch angle vs the flow velocity for the no-freeplay case. The theoretical calculation used three sets of initial conditions, that is, I.C.1, I.C.2, and I.C.3. As described before, the theoretical results are independent of the initial condition. As shown in Fig. 25, the experimental acceleration amplitude is higher than the theoretical results. The acceleration signal response is sensitive to the wind-tunnel turbulence, and this sensitivity increases as the flow velocity increases. The agreement between the theory and experiment near the flutter velocity is good, but for higher flow velocity the agreement is unacceptable. This is consistent with previous work on the wing alone where it was found that a von Kármán plate is not adequate for LCO much beyond the flutter speed,[23] but a higher-order structural theory has been shown to give improved agreement between theory and experiment.[17] Also note that the experimental initial conditions are difficult to determine precisely, and there is some sensitivity to those as well.

Figures 26a and 26b show the theoretical and experimental LCO acceleration amplitude at the wing midspan vs the flow velocity for $d = 0.5$ and 1, respectively. The theoretical calculation used three

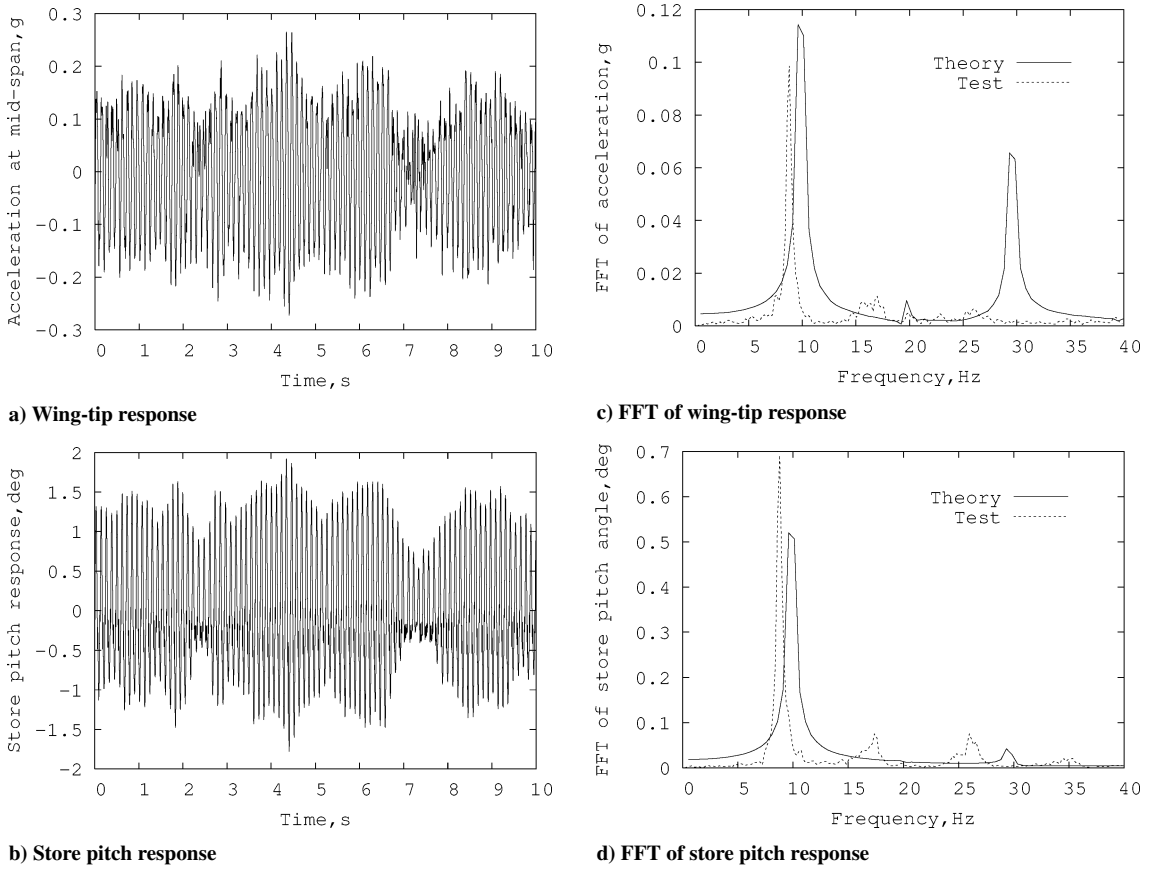

a) Wing-tip response

c) FFT of wing-tip response

b) Store pitch response

d) FFT of store pitch response

Fig. 23 Measured LCO acceleration at midspan of the wing and also the store pitch responses plus corresponding FFT analyses for $U = 26.3$ m/s and $d = 0.5$.

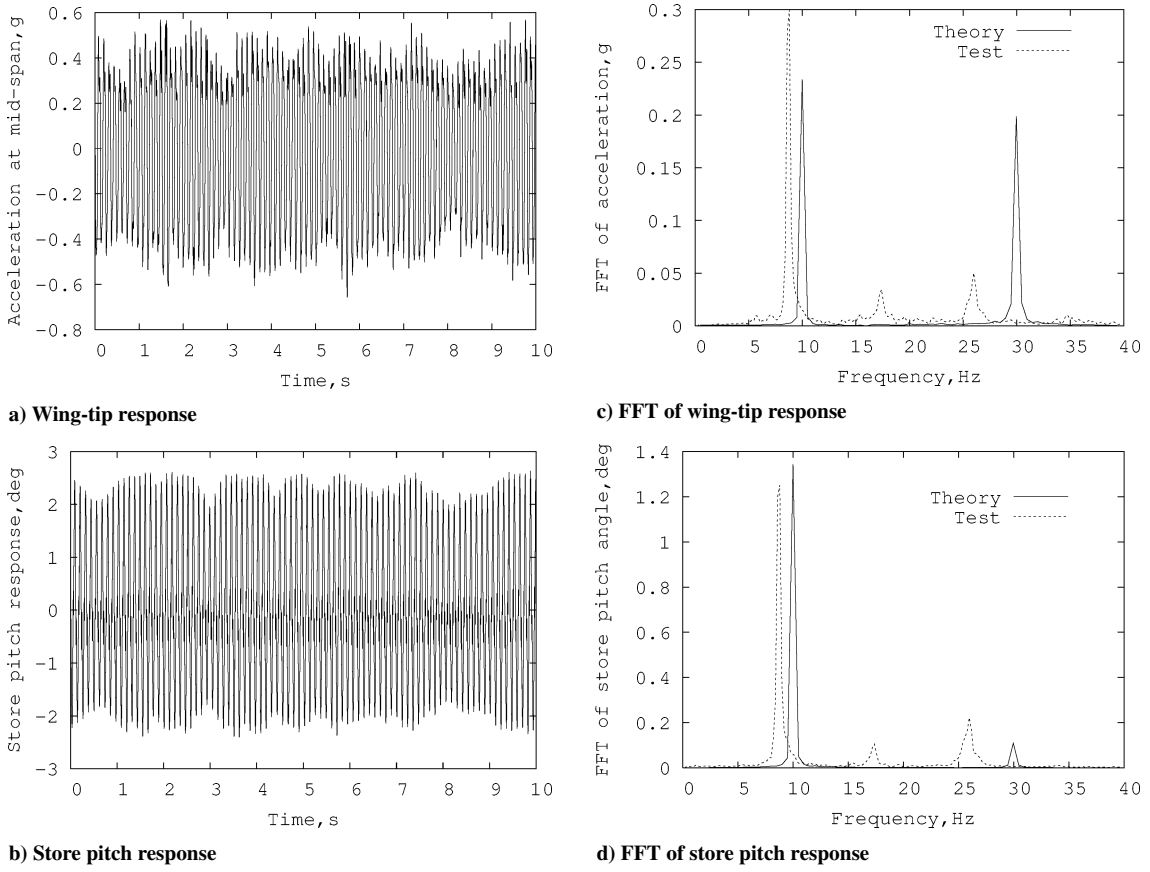

a) Wing-tip response

c) FFT of wing-tip response

b) Store pitch response

d) FFT of store pitch response

Fig. 24 Measured LCO acceleration at midspan of the wing and also the store pitch responses along with corresponding FFT analyses for $U = 25.98$ m/s and $d = 1.0$.

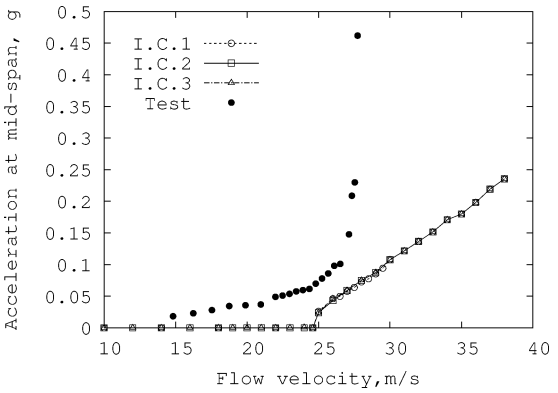

a) Wing-tip response

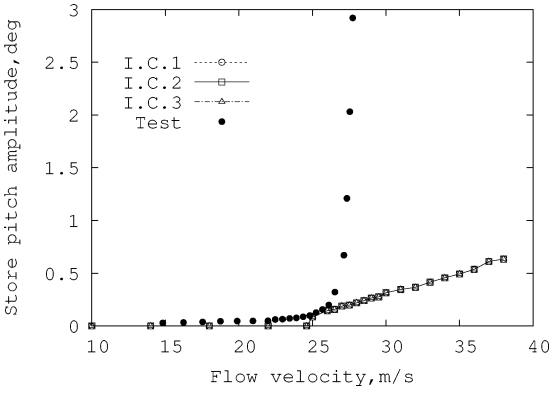

b) Store pitch response

Fig. 25 LCO acceleration amplitude at the wing midspan and the store pitch responses vs flow velocity for no freeplay, $d = 0$.

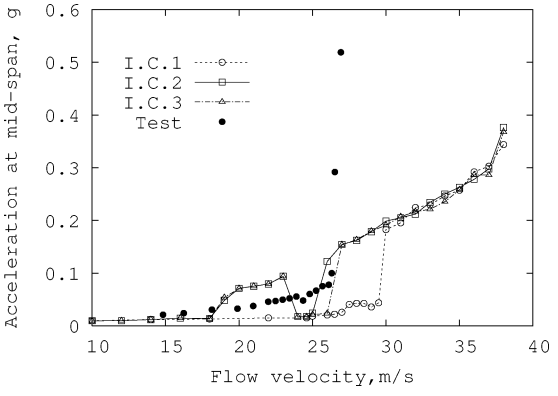

a) $d = 0.5$

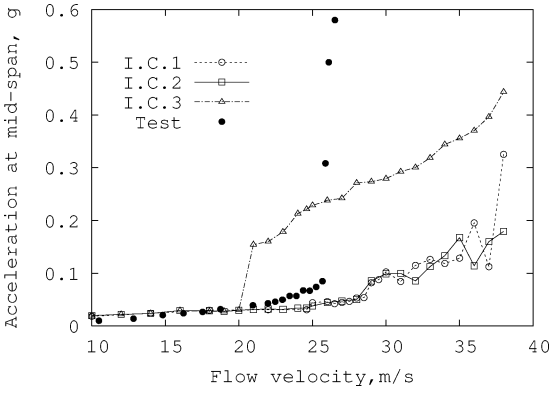

b) $d = 1.0$

Fig. 26 LCO acceleration amplitude at the wing midspan vs flow velocity for two freeplay gaps, $d = 0.5$ and 1.0.

sets of initial conditions, that is, I.C.1, I.C.2, and I.C.3. As described before, the theoretical results are very sensitive to the initial conditions. As shown in Fig. 26, reasonable good agreement between the theory and experiment occurs in the range of $U = 10$–26.5 m/s. However, when the flow velocity is higher 26.5 m/s, the correlation is poor. From these results, two key points are noted:

1) The theoretical model needs to be improved for the structural and possibly the aerodynamic models. An improved structural model has been considered in Ref. 17.

2) A device to more precisely control the initial conditions is needed for wind-tunnel testing of this configuration.

VI. Conclusions

Flutter and LCO of a delta wing with an external store model are studied using von Kármán plate theory, a component modal analysis, and a three-dimensional time-domain linear vortex-lattice aerodynamic model including a reduced-order model aerodynamic technique. Results are computed for different freeplay gap values and store span locations.

The wing-tip LCO amplitude is significantly dependent on the store pitch motion and initial conditions. The LCO behavior is also sensitive to the freeplay gap value and the store span location. When the store is near the wing tip, the freeplay nonlinearity can delay the onset of large-amplitude LCO compared to the no-freeplay case. This is because the effects of store inertia and aerodynamics become significant. In general, the LCO amplitude of the wing tip with freeplay is smaller than that for the no freeplay when the store pitch vibration is small, that is, LCO occurs around only one equilibrium position. However, when the store pitch vibration is large, that is, occurs around two equilibrium positions, the wing-tip LCO amplitude will be larger with freeplay than for the no-freeplay case.

When the wing and store pitch initial conditions are large, the LCO amplitude in the preflutter range can become larger and depends sensitively upon the combination of initial conditions and flow velocity.

The theoretical results have also been compared to experiment for both flutter and LCO. The quantitative correlations for flutter and LCO between the theory and experiment are reasonably good in the range near the flutter velocity, but is poor at the higher flow velocities. It is apparent that the theoretical model needs to be improved using a higher-order structural model as described in Ref. 17.

Acknowledgments

This work was supported under Air Force Office of Scientific Research Grant, "Dynamic and Control of Nonlinear Fluid Structure Interaction" under the direction of Dean Mook and Clark Allred.

References

[1]Lee, B. H. K., Price, S. J., and Wong, Y. S., "Nonlinear Aeroelastic Analysis of Airfoils: Bifurcation and Chaos," *Progress in Aerospace Science*, Vol. 35, No. 3, 1999, pp. 205–334.

[2]Bayly, P. V., and Virgin, L. N., "Chaotic Rattling of a Piecewise Nonlinear Oscillator," American Society of Mechanical Engineers, 91-WA-DSC-17, Dec. 1991.

[3]Liu, L., Wong, Y. S., and Lee, B. H. K., "Nonlinear Aeroelastic Analysis Using the Point Transformation Method, Part 1 and Part 2," *Journal of Sound and Vibration,* Vol. 253, No. 2, 2002, pp. 447–483.

[4]Pitt, D. M., "A Physical Explanation of Freeplay Effects on the Flutter Response of an All-Movable Control Surface," AIAA Paper 95-1387, April 1995.

[5]Henon, M., "On the Numerical Computation of Poincaré Maps," *Physica*, Vol. 5D, No. 5, 1982, pp. 412–414.

[6]Yang, Z. C., and Zhao, L. C., "Analysis of Limit Cycle Flutter of an Airfoil in Incompressible Flow," *Journal of Sound and Vibration*, Vol. 123, No. 1, 1988, pp. 1–13.

[7]Tang, D. M., and Dowell, E. H., "Flutter and Stall Response of Helicopter Blade with Structural Nonlinearity," *Journal of Aircraft*, Vol. 29, No. 5, 1992, pp. 953–960.

[8]Tang, D. M., and Dowell, E. H., "Experimental and Theoretical Study for Nonlinear Aeroelastic Behavior of a Flexible Rotor Blade," *AIAA Journal*, Vol. 31, No. 6, 1993, pp. 1133–1142.

[9]Edwards, J. W., Ashley, H., and Breakwell, J. V., "Unsteady Aerodynamic Modeling for Arbitrary Motions," *AIAA Journal*, Vol. 17, No. 2, 1979, pp. 365–374.

[10]Conner, M. C., Tang, D. M., Dowell, E. H., and Virgin, L. N., "Nonlinear Behavior of a Typical Airfoil Section with Control Surface Freeplay: A Numerical and Experimental Study," *Journal of Fluids and Structures*, Vol. 11, No. 1, 1997, pp. 89–112.

[11]Tang, D. M., Dowell, E. H., and Virgin, L. N., "Limit Cycle Behavior of an Airfoil with a Control Surface," *Journal of Fluids and Structures*, Vol. 12, No. 7, 1998, pp. 839–858.

[12]Denegri, C. M., Jr., "Limit Cycle Oscillation Flight Test Results of a Fighter with External Stores," *Journal of Aircraft*, Vol. 37, No. 5, 2000, pp. 761–769.

[13]Dowell, E. H., and Tang, D. M., *Dynamics of Very High Dimensional Systems*, Component Modal Analysis, World Scientific Publishing, Singapore, 2003, Chap. 10.

[14]Tongue, B. H., and Dowell, E. H., "Component Mode Analysis of Nonlinear, Nonconservative Systems," *Journal of Applied Mechanics*, Vol. 50, March 1983, pp. 204–209.

[15]Dowell, E. H., and Hall, K. C., "Modeling of Fluid-Structure Interaction," Invited Chapter, *Annual Reviews of Fluid Mechanics*, Vol. 33, 2001, pp. 445–490.

[16]Tang, D. M., Attar, P. J., and Dowell, E. H., "Flutter/LCO Analysis and Experiment for a Wing-Store Model, Part I: with von Karman Plate Theory," *AIAA Journal* (submitted for publication).

[17]Attar, P. J., Dowell, E. H., and White, J. R., "Modeling the LCO of a Delta Wing Using a High Fidelity Structural Model," AIAA Paper 2004-1692, April 2004.

[18]Yang, Y. R., and Zhao, L. C., "Subharmonic Bifurcation Analysis of Wing with Store Flutter," *Journal of Sound and Vibration*, Vol. 157, No. 3, 1992, pp. 477–484.

[19]Liu, J. K., and Chan, H. C., "Limit Cycle Oscillations of Wing with Store Flutter," *Journal of Aircraft* (submitted for publication).

[20]Thompson, D. E., Jr., and Strganac, T. W., "Nonlinear Analysis of Store-Induced Limit Cycle Oscillations," *Nonlinear Dynamics* (to be published).

[21]Beran, P. S., Strganac, T. W., Kim, K., and Nichkawde, C., "Studies of Store-Induced Limit Cycle Oscillations Using a Model with Full System Nonlinearities," *Nonlinear Dynamics* (to be published).

[22]Bisplinghoff, R. L., Ashley, H., and Halfman, R. L., *Aeroelasticity*, Addison Wesley Longman, Cambridge, MA, 1955, pp. 418–430.

[23]Tang, D. M., Herry, J. K., and Dowell, E. H., "Limit Cycle Oscillations of Delta Wing Models in Low Subsonic Flow," *AIAA Journal*, Vol. 37, No. 11, 1999, pp. 1355–1362.